



PONTIFICIA UNIVERSIDAD CATOLICA DE CHILE
ESCUELA DE INGENIERIA

**3D MODELING OF DYNAMIC SOIL-
STRUCTURE INTERACTION IN SHEAR
WALL BUILDINGS WITH BASEMENTS
IN MEDIUM STIFFNESS SANDY SOILS
USING SPECTRAL ELEMENT METHOD.
THE CASE OF VIÑA DEL MAR, CHILE**

FELIPE ESTEBAN AYALA SANHUEZA

Thesis submitted to the Office of Research and Graduate Studies in
partial fulfillment of the requirements for the Degree of Master of
Science in Engineering

Advisor:

ESTEBAN SÁEZ ROBERT

Santiago de Chile, (December, 2020)

© 2020, Felipe Ayala Sanhueza



PONTIFICIA UNIVERSIDAD CATOLICA DE CHILE
ESCUELA DE INGENIERIA

**3D MODELING OF DYNAMIC SOIL-
STRUCTURE INTERACTION IN SHEAR
WALL BUILDINGS WITH BASEMENTS
IN MEDIUM STIFFNESS SANDY SOILS
USING SPECTRAL ELEMENT METHOD.
THE CASE OF VIÑA DEL MAR, CHILE**

FELIPE ESTEBAN AYALA SANHUEZA

Members of the Committee:

ESTEBAN SÁEZ ROBERT

DocuSigned by:

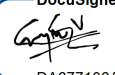
5D7D2E96D73B454...

JOSÉ LUIS ALMAZÁN CAMPILLAY

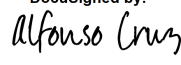
DocuSigned by:

17A77B2E76A8412...

CAROLINA MAGNA-VERDUGO

DocuSigned by:

DA677106A4B143E...

ALFONSO CRUZ NOVOA

DocuSigned by:

2B6660EF50D9427...

Thesis submitted to the Office of Research and Graduate Studies in partial fulfillment of the requirements for the Degree of Master of Science in Engineering

Santiago de Chile, (December, 2020)

To Julita, my beloved grannie.

“Nothing in life is to be feared, it is only to be understood. Now is the time to understand more, so that we may fear less.”

Marie Curie

ACKNOWLEDGMENTS

This investigation is based on work supported by the FONDEF project D10E1027 and by CIGIDEN (National Research Center of Integrated Natural Disaster Management) FONDAP 15110017. We also wish to thank DICTUC for providing the equipment used in the geophysical campaigns.

I certainly can't describe with proper words how grateful I feel for life and every person that has been part of my biography. No matter how hard one can try to succeed, without family, friends, colleagues, acquaintances, and assertive guidance is almost impossible to accomplish anything notable. Special thanks to my advisor, Esteban, who somehow always believed in me and gave me the utmost and seldom found support during these last four years.

Stay motivated, keep up your epic work, and never quit. Remember that whatever you do in this life, it's not legendary unless your friends are there to see it.

GENERAL INDEX

	Page
ACKNOWLEDGMENTS.....	iv
LIST OF TABLES	vii
LIST OF FIGURES.....	viii
RESUMEN.....	xi
ABSTRACT	xii
1. INTRODUCTION	1
1.1 Hypothesis.....	2
1.2 Objectives.....	2
1.3 Literature review	3
1.3.1 Observed damage in RC Chilean buildings.....	3
1.3.2 Soil-structure interaction.....	5
1.3.3 Operational Modal Analysis	7
1.3.4 Spectral Element Method.....	8
1.4 Methodology	10
1.4.1 General strategy	10
1.4.2 Micro-vibrations surveys	11
1.4.3 Calibration of the model	17
1.5 Principal findings and future work.....	21
2. COMPUTATIONAL MODELING OF DYNAMIC SOIL-STRUCTURE INTERACTION IN SHEAR WALL BUILDINGS WITH BASEMENTS IN MEDIUM STIFFNESS SANDY SOILS BY A SUBDOMAIN SPECTRAL ELEMENT APPROACH CALIBRATED BY MICRO-VIBRATIONS.....	25
2.1 Introduction.....	25
2.2 Methodology	29
2.2.1 Chilean building typologies.....	29
2.2.2 Soil-structure model.....	31

2.2.3	Micro-vibrations analysis	32
2.3	Structure and soil modeling	34
2.3.1.	Operational Modal Analysis (OMA) and modal optimization	34
2.3.2.	Geotechnical characterization.....	37
2.3.3.	Seismic inputs	40
2.4	14-story RC Building (E14)	42
2.4.1	Background.....	42
2.4.2	Micro-vibrations analysis	43
2.4.3	Coupled DGSE model	45
2.5	22-story RC Building (E22)	49
2.5.1	Background.....	49
2.5.2	Micro-vibrations analysis	50
2.5.3	Coupled DGSE model	52
2.6	Results	55
2.6.1	Ground Motion and soil.....	57
2.6.2	Structural response.....	61
2.7	Conclusions	69
2.8	Acknowledgements	72
REFERENCES.....		73

LIST OF TABLES

	Page
Table 2-1: Arrays summary. S- n indicates the instrument number, F.F. stands for free field, -1 is the basement level and N-A/B denomination refers to N -th floor slab, A or B location.....	44
Table 2-2: E14 optimization results. Modal shape of the 3 rd mode could not be properly estimated.	47
Table 2-3: E14 DGSE model materials ranges.	47
Table 2-4: Arrays summary. S- n indicates the instrument number, F.F. stands for free field, -4 is the 4 th basement and N-A/B/C denomination refers to N -th floor slab, A, B, or C location.	51
Table 2-5: E22 optimization results. Modal shapes of (*) frequencies could not be estimated.	54
Table 2-6: E22 DGSE model materials.....	54

LIST OF FIGURES

	Page
Figure 1-1: Damage in ground floor observed in Viña del Mar (Bonelli, 2010).	5
Figure 1-2: Sensors location in E14 building surveys (#n denotes the number of the 3D array and RS stands for reference sensors).	15
Figure 1-3: Sensor placed in a subterranean level (left) and buried in a neighbor site next to the building to measure a free field signal (right).	15
Figure 1-4: Sensor placed at a corner of E22 building block.	16
Figure 1-5: Schematic plan view of the triangular array of sensors in E14 site (left) and predominant period results (right).	17
Figure 1-6: Exploration results of best ratio between weighting factors (β/α) in E14. Normalized error allows to compare the magnitude of error between different runs (left), while the right graph shows the ratio (%) between frequency and modal shape components of error for each run.	19
Figure 1-7: Example of LEQ convergence of shear modulus degradation (G) and damping (D) curves in E22 site. The number of iteration (k) is presented along with the number of soil elements that have not met the convergence tolerance (5%).	21
Figure 2-1: E14 (red) and E22 (green) building locations in Viña del Mar. Blue marker indicates the location of VC seismic station (left). Seismograph installed on a 2nd floor slab (right).	29
Figure 2-2: An overview of soil and structure modeling strategy.	33
Figure 2-3: (a) R05-5 and (b) R02-2 Ricker wavelets. (c) Pseudo-spectral acceleration of synthetic motion and available records of 1985 Chilean Earthquake. (d) Normalized	

Fourier Amplitude Spectrum of the seismic inputs. Rectangles indicate identified modal frequencies range of both buildings in red (E14) and blue (E22). Estimated predominant site's period is also shown.....	41
Figure 2-4: (a) Seismographs location on 2nd to 14th floor slabs. (b) Structural model. Dimensions are in meters.	43
Figure 2-5: X-axis (EW) empirical modal shapes (a: $f = 1.8$ Hz, b: $f = 7.69$ Hz). Identified modal frequencies are shown in (c).	44
Figure 2-6: Empirical (black) and theoretical E14 modal shapes, prior (red) and after (blue) optimization (left: x -axis, right: y -axis). Markers: 1 st (x), 2 nd (+), 4 th (o), and 5 th (∇) mode.	46
Figure 2-7: Coupled 3D model. Dimensions are in meters (left: E14, right: E22).	48
Figure 2-8: (a) Seismographs location on 2nd to 20th floor slabs. (b) Tower and (c) Structural model including the parking building. Dimensions are in meters.	50
Figure 2-9: Y-axis (NS) empirical modal shapes (a: $f = 0.8$ Hz, b: $f = 2.82$ Hz). Identified modal frequencies are shown in (c).	51
Figure 2-10: Empirical (black) and theoretical E22 modal shapes, prior (red) and after (blue) optimization (left: x -axis, right: y -axis). Markers: 1 st (x), 2 nd (+), 4 th (o), and 5 th (∇) mode.	53
Figure 2-11: (a) Coupled 3D Model (S3D) and column of soil (S1D). Free field (FF) and foundation input motions (FIM) are extracted and applied over uncoupled structures models M1 (b) and M2 (c).	57
Figure 2-12: Free field PGA of E14 loaded in x -axis (left: R05-5, right: R02-2).....	59
Figure 2-13: Free field PGA of E22 loaded in x -axis (left: R05-5, right: R02-2).....	59

Figure 2-14: Columns of E14-S3D vs. S1D in x -axis (left: R05-5, right: R02-2).....	60
Figure 2-15: Columns of E22-S3D vs. S1D in x -axis (left: R05-5, right: R02-2).....	60
Figure 2-16: Pseudo-spectral acceleration of building base (point D) and free surface motions (point B), loaded in x -axis (left: R05-5, right: R02-2). Predominant elastic soil (S_{14} and S_{22}) and fixed base building (E_{14} and E_{22}) periods are also shown.	61
Figure 2-17: Spectral Ratio between building top and base. Initial elastic model (S3De) is compared against S3D LEQ and uncoupled models (left: E14 EW, right: E22 NS).....	62
Figure 2-18: Vertical displacements snapshots of E14 building base slab under R02-2 action (a: EW, b: NS). Tower typical floor dimensions are 17 m (EW) by 19 m (NS)...	64
Figure 2-19: E14 Interstory drifts (left: R05-5, right: R02-2).....	65
Figure 2-20: E14 Story shear coefficient (left: R05-5, right: R02-2).	67
Figure 2-21: E22 Interstory drifts (left: R05-5, right: R02-2).....	68
Figure 2-22: E22 Story shear coefficient (left: R05-5, right: R02-2).	69

RESUMEN

Se presenta una estrategia de modelación de la interacción dinámica suelo-estructura (DSSI) utilizando el método de elementos espectrales (SEM) con un enfoque Galerkin discontinuo. Se desarrollan modelos estructurales de dos edificios de muros de corte con subterráneos en suelos arenosos medianamente densos. Se realizan mediciones de vibraciones ambientales, utilizando arreglos tridimensionales de múltiples sensores sísmicos, a fin de estimar la respuesta modal empírica y calibrar el subdominio estructural. Posteriormente, se lleva a cabo un proceso de optimización para calibrar modelos volumétricos de las estructuras. Esta optimización se realiza preservando las frecuencias y formas modales más relevantes, para lograr una respuesta dinámica equivalente. Una vez calibrados los modelos estructurales, se ubican sobre un subdominio de suelo y se evalúan parámetros ingenieriles relevantes mediante simulaciones de modelos sometidos a una excitación de onda plana, aproximando el comportamiento no lineal del suelo mediante un enfoque lineal equivalente. En general, los resultados indican que la DSSI causa efectos significativos en la respuesta estructural y depende en gran medida del contenido en frecuencia del input. La inclusión de la DSSI está relacionada con una reducción de las derivas de entrepiso al ser corregidas por el *rocking* de la losa de fundación, que incluye su flexibilidad, además de elongación del período de la estructura, y una disminución significativa del corte de piso en comparación con la respuesta inducida en los modelos de base fija.

Palabras claves: interacción suelo-estructura, micro-vibraciones, SEM, edificios de mros.

ABSTRACT

A modeling strategy of dynamic soil-structure interaction (DSSI) is presented using the spectral element method (SEM) with a Discontinuous Galerkin approach. Structural models of two shear wall buildings with basements in medium dense sandy soils are developed. Measurements of environmental vibrations are executed, using convenient 3D arrays of multiple seismic sensors, to estimate empirical modal characteristics and calibrate accordingly the structural subdomain and low-strain site properties. Afterward, an optimization process is conducted to calibrate volumetric models of structures. This optimization is performed by preserving the most relevant modal frequencies and shapes, to achieve an equivalent dynamic response. Once calibrated, structural models are placed into a neighboring soil model (soil sub-domain), relevant engineering parameters of performance are assessed via simulations of buildings subjected to a plane wave excitation, approximating non-linear soil behavior by equivalent linear strategy. In general, results indicate that DSSI could have significant effects on the structural response and is strongly dependent on input frequency content. Inclusion of DSSI is related to a reduction of interstory drifts if they are properly corrected by the foundation slab rocking, which includes its flexibility, important period lengthening of the structure, and a significant decrease in story shear compared to fixed base referential responses.

Keywords: soil-structure interaction, micro-vibrations, SEM, shear wall buildings.

1. INTRODUCTION

The Central part of Chile has experienced two major earthquakes in 25 years (1985 M_s 7.8 and 2010 M_w 8.8). This region has also the most densely populated cities in the country (Santiago, Viña del Mar and Concepción) and presents one of the largest seismicity in the world, with a return period of 83 ± 9 years for great shocks (Comte, et al., 1986). Accordingly, Chilean practice of design has led to high-density reinforced concrete (RC) shear wall to be the lateral load-resisting and gravity load-bearing system by default in residential buildings over four stories (Moroni & Ghomez, 2002; Massone, et al., 2012). Economic development in main Chilean cities demands taller buildings and more parking levels than ever. Nowadays, it is almost unconceivable the construction of a building without, at least, one basement level. Besides, coastal cities like Viña del Mar and Concepción are important cases of study because unlike Santiago, they present medium stiffness soils and a shallow groundwater table. Indeed, in cities like Santiago, buildings with 4 or more subterranean levels have been built for many years, however the construction of buildings with multiple basements on saturated medium stiff soils is recent.

Current Chilean design approach, in general, is based on a fixed base method and neglects the effects of adjacent lateral soil. However, the response of the soil affects the structural response, and vice versa. This kind of interaction is studied by the dynamic soil-structure interaction (DSSI) and could become more relevant in constructions with several subterranean levels. The aim of the present work is to

determine if DSSI analysis is critical in residential building with basement in medium stiffness sandy soils based on two case studies of Chilean buildings located in Viña del Mar, using a spectral element method (SEM) approach.

1.1 Hypothesis

Dynamic soil-structure interaction (DSSI) plays a significant role in shear wall dominant buildings with basements supported on medium stiffness soils. Neglecting DSSI could lead to non-conservative seismic design, and its effects can be evaluated in a computational 3D model integrating soil and structure domains.

1.2 Objectives

The general aim is to study the effects of dynamic soil-structure interaction in buildings with subterranean levels in medium stiffness soils and to evaluate the influence of soil non-linearity over the structural response, considering typical Chilean building typologies. Specific objectives are the following:

- Conduct micro-vibrations surveys in two shear wall dominant buildings and sites located in Viña del Mar city.
- Analyze data from buildings and sites and estimate their dynamic empirical properties.
- Develop, calibrate and optimize fixed base structural models.
- Develop fully coupled and calibrated 3D soil-structure models (S3D) and compute seismic wave propagation using synthetic input motions.

- Assess the modification of ground motion and soil effects in S3D and compare with uncoupled soil models.
- Compute the structural response in S3D and compare with uncoupled approaches including fixed base structural models.

1.3 Literature review

1.3.1 Observed damage in RC Chilean buildings

Santiago, Viña del Mar and Concepción are three main cities of Central Chile that were notably impacted by the 2010 M_w 8.8 Maule earthquake. Although most buildings performed successfully, Wallace et. al (2012) reported that about 2% of recent RC building stock -constructed between 1985 and 2009, with 9 or more stories- presented severe damage. This major event caused significant damage to RC structural walls, especially near ground level i.e. first floor or first basement level. Observations include flexural compression and brittle shear failures, crushing and spalling of concrete, and concentrated damage due to buckling of vertical reinforcement. Massone et. al (2012) described that affected walls exhibited large spacing of horizontal web reinforcement and hoops (about 20 cm both), and 90° hooks. Besides, spalling of cover concrete (about 4 cm considering both sides) represented a decrease of 20 to 27% of wall thickness in many thin walls (15-20 cm thick). Buckling of vertical reinforcement is, therefore, associated with large spacing of transverse bars and the opening of ineffective 90° hooks, once the cover concrete was broken away.

Multiple cases of damage were reported in areas of abrupt change in wall cross section, typically required by design to place parking spaces, door openings, among others. This effect is associated with stress and strain concentrations around the vertical irregularity.

Jünemann (2015), after studying 36 buildings damaged during the 2010 Maule earthquake, concluded that even though they presented a high average wall density, three critical aspects were reported: smaller wall thickness, larger axial loads, and larger vertical irregularities concentrated in lower levels, when compared to common buildings affected by 1985 event.

Lagos et. al (2012) highlighted that even though Performance Based Design is not included in the Chilean seismic design code, the 2010 experience showed that Chilean RC buildings in general responded close to operational performance level. And for frequent and occasional earthquakes, Chilean buildings response is essentially elastic and have fully operational performance.

Regarding the city of study, Carpenter (2011) pointed out that in Viña del Mar damaged buildings were clustered in a zone with higher level of demand than anticipated in geotechnical characterization. Structural design may have used a soil condition based on upper sandy soils and neglected amplification effects due to the thickness of these deposits. Indeed, Podestá (2019) reported that most damaged buildings presented a fundamental period very close to site predominant period, so severe damage could be more related to site-structure resonance rather singular site-

amplification effects. Figure 1-1 shows important damage reported in Viña del Mar, in RC buildings structural walls of ground level.



Figure 1-1: Damage in ground floor observed in Viña del Mar (Bonelli, 2010).

1.3.2 Soil-structure interaction

The study of dynamic soil-structure interaction (DSSI) corresponds to the analysis of the effects of the foundation soil on the dynamic response of a structure, but also of the influence that the building has on the dynamic behavior of the soil. This interaction depends on various factors such as soil characteristics, structural system, and type of foundation. In some situations, such as in the case of certain types of structures founded on the surface, DSSI effects can be neglected. In other cases, such as dams, nuclear power plants, large storage ponds, bridge piers or other slender structures, the effects of DSSI can be important and should be incorporated into the design.

Although the deformation range of dynamic elastic behavior of the soil is very small, historical studies by DSSI (Jennings & Bielak, 1973; Veletsos & Meek, 1974; Veletsos & Nair, 1975) have been carried out under the hypothesis of elastic behavior of both the soil and the structure. This hypothesis is rooted in the limitations of the usual techniques to develop a realistic analysis of the inelastic phenomena. Indeed, the evaluation of inelastic effects is currently a subject of active research. The mechanisms of DSSI are classically explained by two physical phenomena: inertial interaction and kinematic interaction (Kausel, 2010). Inertial interaction groups the effects of the vibrating structure over the soil-foundation interface in terms of displacements and rotations. This in turn is reflected in energy dissipation via radiation damping and hysteretic soil damping. In consequence, with DSSI the overall system increases in flexibility (building period lengthening) and damping. On the other hand, kinematic effects refer to the modification of foundation motions through three main contributions: base-slab averaging, embedment effects, and wave scattering, under the assumption of foundation inertia absence (Stewart, Seed, & Fenves, 1998).

In the case of buildings with subterranean levels, a relevant question to address is the pertinency of the input motion used in structural design and simulations. Usually earthquakes are recorded under the free field condition (i.e. there is no significant effect of structures over the recorded ground motion). According to Stewart & Tileyliglu (2007), current practice fails to represent adequately several characteristics of the actual excitation in the base of the building: reduction of

translational components with depth, rocking components of base motion, and effects of DSSI over basement perimeter walls and base slabs.

Regardless the approach selected to study the soil-structure interaction problem (direct analysis, sub-structuring method and fixed base), it is clear that implementation of DSSI requires collaboration between structural and geotechnical engineers, being the case that neither discipline alone is expected to assess properly the variety of effects and complexities required for an appropriate DSSI analysis. Further references and related work can be found in Chapter 2.

1.3.3 Operational Modal Analysis

The dynamic identification using ambient vibrations represents an attractive alternative in the system identification of modal properties of existing structures, since it does not require excitation equipment and the tests are performed during the normal use of the structure. The identification of dynamic parameters of existing structures has many applications: model updating, damage assessment, structural health monitoring, among others.

Traditionally in the system identification, input (excitation) and output (response) data were used to estimate the dynamic parameters of the structure. Based on the concept of the input-output (I/O) relation, numerous identification techniques or methods were developed in the domain of time and frequency. However, this traditional approach, known as Experimental Modal Analysis (EMA), has important limitations in the case of large structures, since it is difficult to apply, due to the great

amount of energy required to excite the structures, in addition to the inconvenience of stopping the normal operation to perform the measurements.

On the other hand, system identification with ambient vibrations uses only the response measurements of the structure in operational conditions, so this type of methodology and surveys are cheaper and faster to perform because it does not require equipment to excite the structure or interfere with the normal use of the existing structure. This method, called Operational Modal Analysis (OMA), has been broadly validated (Brincker, Zhang, & Andersen, 2000; Ventura, et al., 2005; Jacobsen, Andersen, & Brincker, 2007; Döhler, Andersen, & Mevel, 2017), and constitutes the approach selected for the present study. Further details about the surveys conducted, processing methods and previous work can be found in the sections below.

1.3.4 Spectral Element Method

Evaluation of the seismic response of realistic 3D models, with irregular topography, internal interfaces, heterogeneous properties and meshing has been actively studied in recent years. The general scope is to develop a fully coupled 3D model able to handle unstructured domains and solve the elastodynamics equations in a reasonable time of computation. Finite difference method (FDM) has been widely used for realistic applications (Frankel, 1993; Olsen & Archuleta, 1996; Pitarka & Irikura, 1996), but experiencing numerical dispersion, problems simulating free-surface condition, and lack of geometrical flexibility. A variation of finite element method (FEM) called domain reduction method (DRM) was implemented by Xu & Bielak

(2003), being capable of evaluate 3D wave fields in highly heterogeneous media (large impedance contrasts and arbitrary interfaces) induced by an arbitrary excitation source.

In the investigation herein, another successful variation of FEM is used to solve the weak formulation of elastodynamics i.e. spectral element method (SEM), which is also known as the N or h - p version of FEM, using high-order interpolants evaluated at the Legendre-Gauss-Lobato (LGL) quadrature points (Komatitsch & Tromp, 1999; Guo & Babuška, 1986). SEM has been originally developed for fluid dynamics (Patera, 1984) and after extended for 3D seismic wave propagation problems (Komatitsch D. , 1997; Faccioli, Maggio, Paolucci, & Quarteroni, 1997; Paolucci, Faccioli, & Maggio, 1999). This technique can handle free-surface topography, accurate surface waves propagation, and parallel computation. It combines the geometrical flexibility of finite element approach and the accuracy of spectral methods.

The Discontinuous Galerkin version of SEM (DGSE) presents great stability when is applied to wave propagation problems, because it presents dispersion and dissipation errors that decrease with exponential order. Additionally, the fact that the transmission of information between elements is imposed in a discontinuous way makes it especially attractive for solving problems with high spatial and material heterogeneity. This non-conforming discretization technique enables geometrical and polynomial flexibility and is used to glue together different subdomains.

In the present study, the subdomains correspond to the apparent bedrock, sandy soils (coarse and fine mesh), and the building. The implementation used to evaluate DSSI effects in the fully coupled 3D models is the open-source numerical code SPectral Elements in Elastodynamics with Discontinuous Galerkin (SPEED), firstly introduced in Mazzieri et al. (2013).

1.4 Methodology

To recreate realistic and fully coupled 3D models of the selected two case studies, a methodology based on ambient micro-vibrations is used. In this approach, several surveys were designed and performed in both sites and buildings. The following subsections describe the main challenges throughout the experimental and subsequent calibration process of the soil-structure dynamic system. This section is divided into three subsections. Firstly, an overview of the case studies and general strategy are presented. Then the experimental stage is detailed. Finally, updating and calibration of the soil-structure model are explained, besides its key features and original developments of this investigation.

1.4.1 General strategy

The selected structures correspond to two shear wall dominant RC buildings with basements, both built on soils of the same geological formation, in Viña del Mar downtown. The first structure is a 14-story residential building with one basement, located about 200 m north of the Marga-Marga river and 700 m west of the coast. The second, meanwhile, is a commercial building with 22 stories and 4 subterranean

levels. It is located approximately 600 m north of the Marga-Marga river and 800 m west of the coast. The building identifications are E14 (14 stories + 1 basement) and E22 (22 stories + 4 basements).

Through the collaboration of private companies (construction and real estate), we accessed structural and architectural drawings of buildings, both in the final stage of construction. With the information collected, models of the structures were developed using a widely known software of structural analysis, as a first approximation to the global dynamic behavior. Subsequently, micro-vibrations surveys were carried out using SARA® SL06 triaxial seismographs.

Once the data is obtained, the experimental dynamic properties of the structure are estimated; in particular, first frequencies and modal shapes are identified using Operational Modal Analysis. Then, an equivalent volumetric model of the structure is calibrated based on the modal results, to be used later in the DSSI analysis. Meanwhile, from the soil measurements, the predominant period of the site is estimated, which allowed, in turn, to adjust the depth of the transition from medium stiffness soil to a stratum of higher stiffness (apparent or seismic bedrock). Finally, with a characterized soil-structure system, a coupled 3D model is built, to assess the soil-structure interaction under a vertically incident plane wave excitation.

1.4.2 Micro-vibrations surveys

All the measurements were performed using different arrays of SARA® SL06 triaxial seismographs. This equipment is used for a wide range of applications: seismology, geophysical surveys, structural health monitoring, and modal

identification. The seismograph can be utilized with a variety of triaxial sensors available in the market. In the study herein the SARA® SS05BH sensor was adapted for its usage on rigid surfaces. It was mounted on a specially designed rigid tripod base with a bubble level. The frequency band of operation of the sensor is 0.5-50 Hz according to the manufacturer, which is enough for the frequency range of Viña del Mar soil deposits and modal analysis of both RC buildings (SARA Electronic Instruments, 2020).

1.4.2.1 Micro-vibrations in buildings

The survey procedure was designed and performed based on recommendations of ARTeMIS user manual and personal communication with one of the developers of this modal extractor software. With the OMA approach selected, a specific strategy to measure ambient vibrations according to each building's specific characteristics was defined. Because of the limited number of available sensors and the number of stories, the multiple *Test Setups* (each *Test Setup* is an array or configuration of sensors) procedure was chosen. In this methodology reference sensors (at least 1) are needed, while the other sensors are moved to different stories of the building, and assuming a white noise input, different configurations can be post-processed as a consolidated single one, covering all the desired positions. Each configuration of sensors (shown in Figure 1-2 for E14) was synchronized via GPS antenna with the UTC standard. Some recommendations are summarized next:

- The verticality of each sensor must be ensured. In this case, a bubble level was used in the rigid tripods.

- The orientation of the sensors is critical in system identification. The north (or reference orientation) of each sensor must be perfectly aligned with the rest of the sensors. Otherwise, analysis of empirical data could lead to physically meaningless results, such as modal shapes that describe e.g. an unrealistic expansion of concrete slabs.
- In each story, it is required to measure at least three horizontal components in two points of the slab (a discernible distance is needed e.g. two corners of the same story or one corner and the floor geometric center) to properly characterize in-plane (horizontal) modes.
- It is strongly recommended to measure at least 20 minutes to obtain adequate ambient data. In this survey, 30 minutes of synchronized data were obtained in each configuration.
- Better data can be obtained if reference sensors are mounted on upper stories, such as the top floor or the rooftop because large amplitude of ambient vibrations. This also allows measuring relevant modes since nodes of modal shapes are generally avoided.
- A perfect synchronization is required to acquire consistent data. Even though a wire connection between sensors is recommended, this is almost inapplicable to most buildings. Moreover, wireless synchronization gives enough flexibility to move sensors to any position without affecting the survey quality.

- In the chosen wireless method of synchronization, GPS antenna, it was necessary to synchronize initially all sensors in an open place (roofless). This step is critical, especially in equipment placed in subterranean levels, due to the absence of a strong GPS signal below ground level.
- The free field sensor should be located at least 20 meters away from the building ground slab. So, the building does not interfere strongly in the kinematics of the free surface recorded signal. Because of the type of sensors that were used, better data was obtained when the free field sensor was a few inches buried (see Figure 1-3).
- It was found that a reasonably good frequency band of operation of instruments for this type of survey is 0.5-15 Hz.

Each decision and design process of the surveys should consider the characteristics of the available equipment. Further details can be found in Chapter 2.

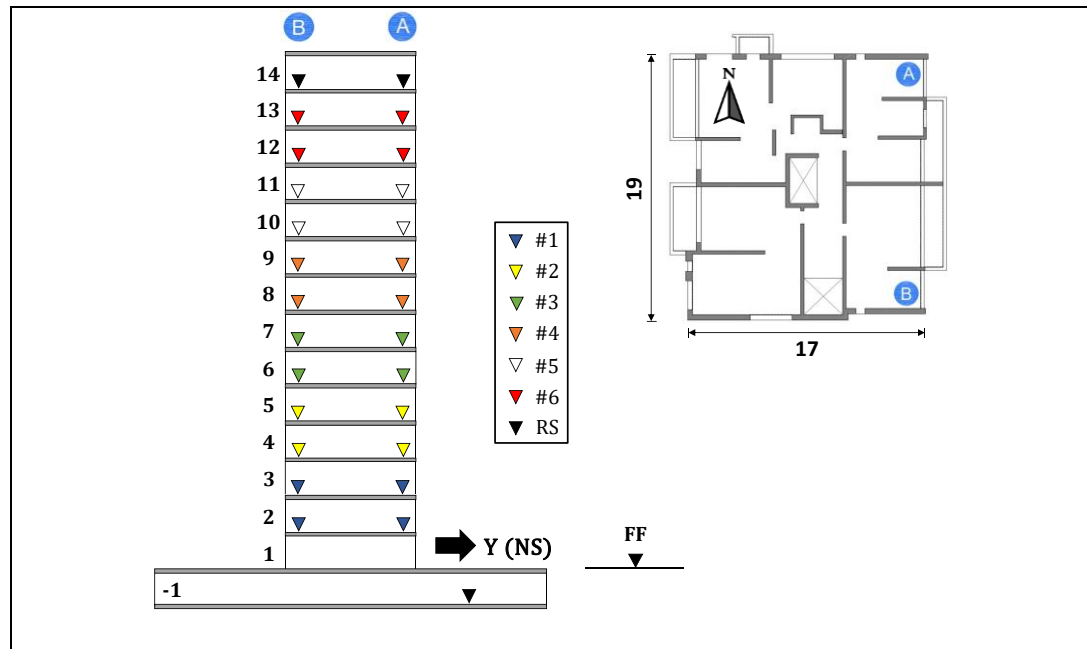


Figure 1-2: Sensors location in E14 building surveys (#**n** denotes the number of the 3D array and **RS** stands for reference sensors).



Figure 1-3: Sensor placed in a subterranean level (left) and buried in a neighbor site next to the building to measure a free field signal (right).

1.4.2.2 Estimation of predominant period of the sites

The Nakamura method (Nakamura, 1989) has been widely recognized as a valid estimation of the global seismic behavior of a soil deposit. It relates the horizontal to vertical spectral ratio (HVSr) of surface microtremor to estimate the predominant period of a site, recorded at a single station. In this investigation, 3 hours of measurements of the site were performed, in a triangular array located at three corners of each building block, synchronized by GPS (Figs. Figure 1-4 and Figure 1-5). The peak of the empirical HVSr allows to identify the predominant period of the site. A higher peak denotes a greater impedance contrast between the soil deposit and the seismic basement (Leyton, et al., 2013). Figure 1-5 shows results of E14 surveys (median curves of HV ratio), and as can be seen, estimated predominant frequencies vary from 1.34 to 1.67 Hz, with a range of amplitude from 2.8 to 4.6.



Figure 1-4: Sensor placed at a corner of E22 building block.

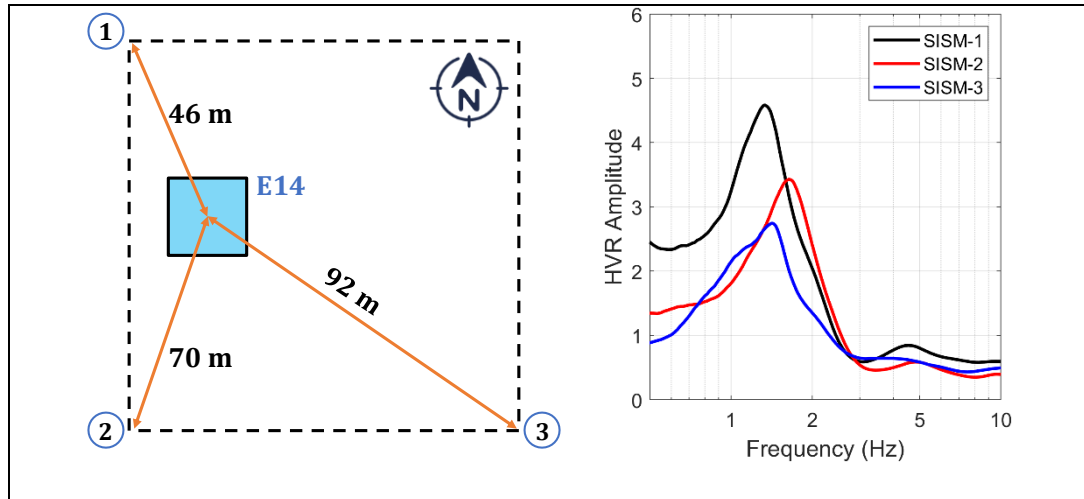


Figure 1-5: Schematic plan view of the triangular array of sensors in E14 site (left) and predominant period results (right).

1.4.3 Calibration of the model

1.4.3.1 Structural model updating

One of the main challenges of the present investigation was to transfer empirical data and subsequent modal properties into a volumetric model. The problem can be approached in several ways, so it was necessary to define some criteria to develop an initial model. The first definition was purely geometrical based on the global dimensions of each building. This initial approach consisted of recreating below ground geometry (subterranean levels), story heights, and plan dimensions of typical floor. The next step was to define the mesh size, that had to be conforming within the building subdomain. Massone et. al (2012) reported that in Chilean buildings, typical RC walls thickness ranges from 15 cm to 30 cm, while typical floor slabs are

about 15 cm to 30 cm thick. Considering this information, an average structural mesh size of 20 cm was firstly chosen. However, because of the Courant-Friedrichs-Levy (CFL) condition over time discretization of the SEM numerical scheme, the resulting required time step for stability was too small and computing time notably increased. After several iterations (and testing the capability of the structural model to recreate empirical modal properties), a minimum mesh size of 50 cm was adopted in both buildings.

Once the mesh was defined, the following goal was to find the best possible fit between empirical and theoretical dynamic properties. Chapter 2 provides details of the minimization problem and multivariable error function, which was implemented using the MATLAB® optimization function *fmincon*. The multivariable error function, is expressed as:

$$e = \sum_i^N \frac{1}{f_{ei}} \left(\alpha \frac{\|\Phi_{ei} - \Phi_{ti}\|}{\|\Phi_{ei}\|} + \beta \frac{|f_{ei} - f_{ti}|}{f_{ei}} \right) \quad (1-1)$$

Where $\{f_{ei}, \Phi_{ei}\}$ and $\{f_{ti}, \Phi_{ti}\}$ are the empirical and theoretical frequencies and modal shapes respectively, α and β are scalar weighting parameters and N is the total number of modes used for the error computation. The minimization problem is:

$$\begin{aligned} & \text{minimize } e & (1-2) \\ & \text{subject to } E_j \geq E_{j+1} \quad \forall j = \{1..n-1\} \end{aligned}$$

Where E_j is the elastic modulus of the j -th set of walls and n is the number of different groups of walls. This optimization algorithm was developed to explore a wide range of weighting factors applied over the error function (specifically the ratio between weighting factors, defined as β/α), in order to find the best values of material parameters minimizing the differences against empirical data. Figure 1-6 shows effects over error after applying a wide range of weighting factors ($\beta/\alpha = 0.01$ -10). The relative error between the frequency and modal shape (Φ) components of the error exhibits a stabilization for β/α higher than 2. As can be seen, in E14 there is a zone ($\beta/\alpha \sim 1.7$ -2.7) that shows lower values of error and a stable ratio between the two error components. It is worth to mention that for values of β/α lower than 1 the dispersion notably increases and the frequency term of the total error rises.

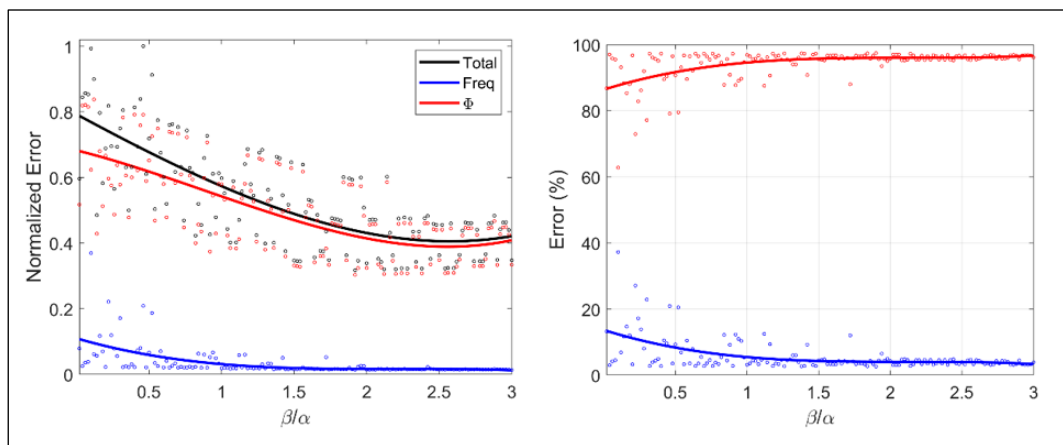


Figure 1-6: Exploration results of best ratio between weighting factors (β/α) in E14. Normalized error allows to compare the magnitude of error between different runs

(left), while the right graph shows the ratio (%) between frequency and modal shape components of error for each run.

In general, optimization results indicated that several sets of parameters led to a reasonably similar error. To choose a model, the following criteria were adopted, so the one that fulfilled more of these criteria was finally chosen:

- 1) Building fundamental frequency (f_1) error below 2%.
- 2) The ratio of the second mode to first mode frequencies (f_2/f_1) error below 8% (E14) and 2% (E22).
- 3) Lowest modal shape error in 1st mode x -axis (E14) and y -axis (E22).
- 4) Lowest modal shape error in 2nd mode x -axis (E14) and y -axis (E22).
- 5) Lowest modal shape error in 4th mode x -axis (E14) and y -axis (E22).
- 6) Lowest modal shape error in 5th mode y -axis (E14) and x -axis (E22).

Criteria 3) to 6) were based on the overall contribution of each mode, computed as the effective modal mass in the analyzed direction. Results of both buildings are presented in Chapter 2.

1.4.3.2 LEQ approach

The non-linear soil behavior is approximated using the Linear Equivalent (LEQ) method. Using an iterative process, shear modulus degradation and damping curves are used to update soil properties, based on the computation of maximum shear strains. This approach is applied in each elastic iteration until convergence, defined by a maximum of 5% difference in the shear modulus (current iteration compared to the previous one). The LEQ method was implemented in the SPEED models, both

in the fully coupled 3D model (S3D) and 1D soil columns (S1D), as part of the input calibration of uncoupled models.

Figure 1-7 shows an example of the convergence process of S1D, applied in E22 site subjected to R02-2 ground motion.

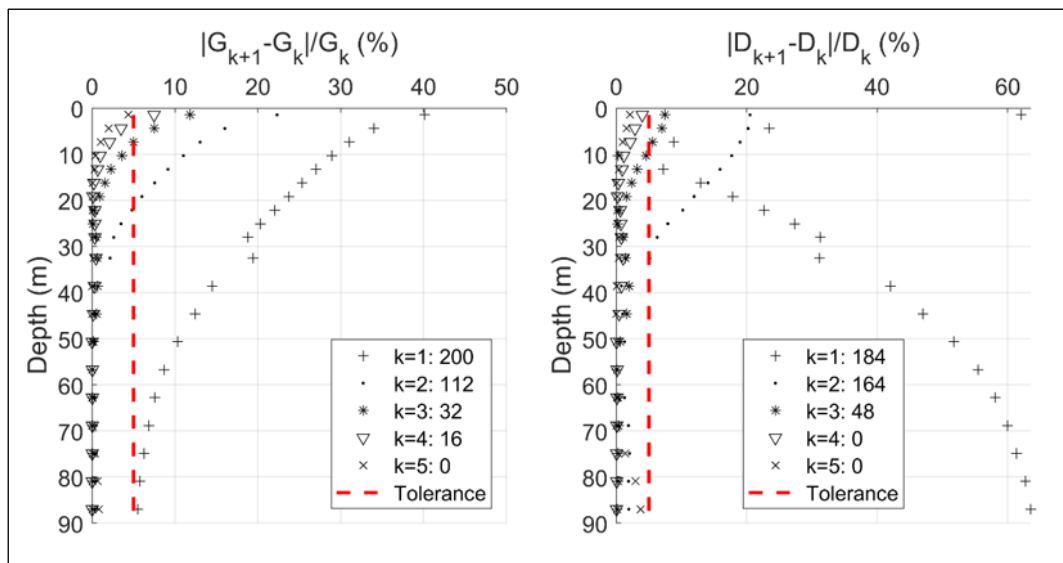


Figure 1-7: Example of LEQ convergence of shear modulus degradation (G) and damping (D) curves in E22 site. The number of iteration (k) is presented along with the number of soil elements that have not met the convergence tolerance (5%).

1.5 Principal findings and future work

This research aimed to develop a methodology to quantify DSSI effects in buildings with subterranean levels, study soil non-linearity effects using the LEQ approach, and compare different modeling approaches to evaluate soil-structure interaction in shear wall dominant buildings on medium stiffness sandy soils. A 3D model for

seismic wave propagation was developed for each building. Two shear wall dominant buildings were simulated in a fully coupled 3D soil-structure model. Also, two fixed base approaches (uncoupled) are studied to compare roof displacements, interstory drifts, story shears, and accelerations.

Based on the selected case studies (shear wall buildings, mat foundation, sandy soils, and Ricker wavelet inputs), the following conclusions can be drawn:

1. The calibration strategy using ambient micro-vibrations was successful. S1D models showed that soil deposits responded in a frequency range that matched the predominant period computed by Nakamura's method. On the other hand, a reasonably good match with target data was obtained in both buildings, especially in modes of vibration with an important dynamic contribution.
2. The selection of adequate ground motion is extremely important. Two characteristics are the most critical: frequency content and location e.g. free field (FF) or foundation input motion (FIM).
3. DSSI results shown, in general, an average response between FF and FIM responses of fixed base models.
4. DSSI induces larger interstory drift demands in subterranean and shallow levels when compared to uncoupled models. However, if drifts are corrected by the base slab rocking, the fully coupled 3D model (S3D) exhibits an intermediate to lower response than fixed base approaches.
5. DSSI generates a significant decrease in story shear envelope compared to FF.

6. Elastic DSSI gives rise to significant period lengthening. This effect is increased if the soil non-linearity is introduced.

Recommendations for future work include:

1. Using real earthquake motions: even though the Ricker inputs were calibrated to cover a wide range of frequencies and to match PGA historical earthquakes, it was a forced modeling decision because of limited computational equipment available. The content and complexities of an actual recorded signal cannot be fully replaced by a synthetic input with a limited duration of a couple of seconds.
2. Non-linear approaches for soil and structure materials: results shown that building response was fundamentally elastic but using stronger and plausible ground motions can certainly induce inelastic incursions of the structure. Regarding the soil, a non-linear method that updates the model in each time step is computationally more expensive, but it certainly offers a comparison framework to validate the selected LEQ approach.
3. Global methods of optimization: the optimization function exhibited a strong dependency on the initial value, so the solution that satisfies the constraints and minimize the objective function is local. Global optimization could allow finding equivalent or better solutions without a good initial combination of parameters, which could be useful in cases where the structural details of the project is not available.
4. The inclusion of soil flexibility in building calibration: the fixed base approach to calibrate the buildings was chosen due to its simplicity, besides allowing to

directly compare later with fixed base approaches. This modeling decision was based on the hypothesis that ambient vibrations induce negligible strains in the soil. Thus, the surrounding soil deposit reasonably fixes the superstructure without adding discernible flexibility to the system. Nevertheless, a sensitivity analysis is needed to confirm this simplified approach.

5. Validation of optimized models against recorded motions from well-instrumented buildings. One feasible option is to compare the phase and amplitude of building roof response during a seismic event. However, for a proper DSSI analysis, sensors are needed to record structural translations at the foundation and roof (at least two vertical sensors on the foundation to record rocking), and a ground instrument near the building.

Further study is required to draw general conclusions about DSSI effects in shear wall dominant buildings. The following article shows the results of the combination of applying two Ricker wavelet inputs using two modeling approaches (fully coupled and uncoupled), in two principal directions (EW and NS) of two shear wall dominant buildings located on medium stiffness sandy soils of Viña del Mar.

2. COMPUTATIONAL MODELING OF DYNAMIC SOIL-STRUCTURE INTERACTION IN SHEAR WALL BUILDINGS WITH BASEMENTS IN MEDIUM STIFFNESS SANDY SOILS BY A SUBDOMAIN SPECTRAL ELEMENT APPROACH CALIBRATED BY MICRO-VIBRATIONS.

2.1 Introduction

When subjected to seismic motions, the response of a structure and the surrounding soil does not depend on its own characteristics separately, but on a mutual influence between them. Thus, the dynamic behavior of the structure depends on the ground and vice versa. This physical phenomenon is denominated dynamic soil-structure interaction (DSSI) and could become more important in moderate to severe earthquakes.

Economic development in main Chilean cities currently demands taller buildings and more parking levels than just a decade ago. This had led to shear wall resisting system with multiple basements, to be the most frequent type of construction throughout the country. Viña del Mar and Concepcion are remarkable cases of study, because both cities present medium stiffness soils and a shallow groundwater table.

There are currently at least three approaches to assess the problem of seismic response of buildings with underground levels: 1) the dynamic sub-structuring method, which uses boundary elements and considers a rigorous treatment of

boundary conditions; 2) the direct method, which considers a fictitious limit or interaction horizon, where a representative border condition is evaluated in an approximate form of the original problem (Wolf, 1985); and 3) the fixed base method, which does not consider the soil-structure interaction and comprises the current design approach of buildings in Chile. Usually, the structure is supposed to be fixed at its base, and the effects of local soil, in general, are approximated in two ways: 1) selection of adequate design spectrum compatible with site classification and 2) a vertical foundations release, which is replaced with elastic springs as a simplification of soil stiffness.

These simplified hypotheses rely on the fact that DSSI analysis has shown favorable effects, resulting in a decrease in the structural seismic demand when compared to the fixed base analysis. Thus, the tradeoff between the complexity of DSSI analysis and the possible reduction of construction costs has not yet been assimilated by the industry. However, in Mylonakis (2000) it is described that DSSI analysis leads to an increase in the fundamental period of the structure and this effect does not ensure a lower response of the dynamic system. Therefore, under certain circumstances, the fixed base design approach might not be conservative. Especially if building modal analysis considers several modes, the subsequent reduction of loads due to elongation of the vibration period does not necessarily affect all the modes in the same way.

Two physical phenomena explain the mechanisms of DSSI: inertial and kinematical interaction (Kausel, 2010). Kinematic effects refer to modification of foundation

motions through three main contributions: base-slab averaging, embedment effects, and wave scattering (Stewart, Seed, & Fenves, 1998). In the case of buildings with basements, there are two important aspects to be issued: the influence of non-linear soil behavior and the effects of the lateral pressures, especially in deep cases, related to several underground levels.

Despite DSSI has been the subject of numerous studies, limited attention has been devoted to shear wall buildings with several underground levels. Balkaya (2012) studied 140 shear wall dominant buildings under four different types of soil and concluded that code-based methods to estimate the period of the structure exhibited erroneous results and mislead DSSI effects. Han (2002) pointed out that fixed base analysis in tall buildings does not represent real seismic response, since structural stiffness is overestimated and damping underestimated. Naeim et al. (2008) reported that DSSI analysis modifies the characteristics of input motions compared to free field, affecting the response of buildings with subterranean levels, and has a significant impact on interstory drifts distribution. This study also concluded that two common approaches i.e. fixation at ground line and fixing at the base level with horizontal springs in basement walls, both with free field inputs, provided poor results in reproducing the observed response in instrumented buildings. Stewart & Tileylioglu (2007) stated that current practice fails to reproduce physical phenomena occurring below ground surface, and the modification of base input motion (reduction of translational components with depth, rocking of base excitation and effects along basement walls and base slabs) is an open problem in buildings with

subterranean levels. Kraus (2013) also pointed out that fixed base analysis might be valid only if the foundation soil has higher relative stiffness than the building since soil deformations at the interface are negligible. Regarding overall structural response, incorporation of DSSI has been reported to be strongly dependent on the type of building and foundation, soil stiffness, and ground motion frequency content (Dutta, Bhattacharya, & Roy, 2004). In fact, several studies of DSSI on structures have presented important variations in ductility requirements, roof displacement, interstory drift and shear, acceleration peaks, and overturning moment (Kutanis & Elmas, 2001; Lu, Chen, Li, & Chen, 2003).

The aim of this study is to provide a methodology to quantify the effects of DSSI in shear wall buildings with underground levels and evaluate the influence of the soil non-linearity over the dynamic response of the structure. The approach followed consists in to combine two volumetric sub-domains by the Spectral Element Method (SEM). A non-conforming discontinuous Galerkin approach is chosen to develop a fully coupled soil-structure model (DGSE). The structural model was calibrated against an experimental modal analysis based on micro-vibrations. The main advantage of using a volumetric approach lies in avoiding detailed building modeling and allowing the use of highly efficient numerical strategies for wave propagation problems such as SEM. Regarding study cases, a 14-story (+1 basement) residential building and a 22-story (+4 basements) commercial building are selected for this study (E14 and E22 denominations will be used). Both structures were built on saturated sandy soils of the same sedimentary valley, in

Viña del Mar downtown. Their approximate locations and the Viña Centro (VC) seismic station are shown in Figure 2-1.



Figure 2-1: E14 (red) and E22 (green) building locations in Viña del Mar. Blue marker indicates the location of VC seismic station (left). Seismograph installed on a 2nd floor slab (right).

2.2 Methodology

2.2.1 Chilean building typologies

In Chile, reinforced concrete (RC) buildings are the predominant buildings over four stories (Wallace, et al., 2012). Chilean medium to high-rise RC residential buildings are characterized by structures typified as shear wall buildings, reaching almost 4/5 of national RC building stock (Gómez, 2001; Calderón, 2007), in contrast to RC frame buildings, usually constructed among other countries of the region. The prevalence of this seismic resistant system relies on its adequate performance in past

severe earthquakes, both serviceability and safety (Magna-Verdugo & Kunnath, 2014). In terms of wall density, Chilean buildings present roughly 3% in each principal direction, resulting in a high number of RC walls per story, when compared, for instance, with U.S. buildings (Massone, et al., 2012). These features are justified by Chilean design requirements, where conservative limits in estimated drift and ductility demand are specified (Guendelman, Guendelman, & Lindenberg, 1997; Lagos, et al., 2012). According to Jünemann (2015) and Massone (2012), the most common typology of residential buildings corresponds to a “fish-bone” configuration, that consists of a central corridor – usually containing the elevators - well defined by parallel RC walls and transverse walls that delimit the apartment areas. This RC walls system is designed to simultaneously resist gravity and lateral loads.

As mentioned before, the two case studies correspond to Chilean plan typologies of RC buildings. Through the collaboration of private construction companies, structural and architectural building drawings were obtained. From the information provided in the design documentation, models of the structures were built using a commercial structural analysis software, as a first approach to assess their global dynamic behavior. As detailed below, we accessed to both buildings during their final stage of construction to perform micro-vibrations measurements.

2.2.2 Soil-structure model

An essential part of this research is to develop an equivalent volumetric finite element model (FEM) of each studied structure, calibrated on empirical modal results. The objective is to develop a model as simple as possible but preserving its main modal properties and to be feasible to include in the DGSE approach considered for this research. Previous work in modal identification techniques and calibration of a structural FEM model has been done using a broad set of elements and parameters. For instance, in Ventura (2005) a methodology is presented to update the properties of a structural FEM model, using vibration data. They worked in two buildings updating several properties (elastic modulus, mass density, moment of inertia, and thickness) including different types of elements: slabs, beams, columns, walls, and cladding panels. In consequence, a reasonably match of experimental modes, using volumetric elements and only updating their elastic modulus, is challenging.

Once the soil and the structure are characterized, a fully coupled 3D model is developed to monitor the soil-structure interaction under a plane wave excitation. Spectral approach has proven to be highly effective in solving 3D seismic wave propagation problems in extremely heterogeneous media (Mazzieri, Stupazzini, Guidotti, & Smerzini, 2013). The SEM is the N-version of the FEM, using high-order interpolants evaluated at the Legendre-Gauss-Lobato (LGL) quadrature points, to represent the finite dimensional space (Komatitsch & Tromp, 1999). This

approach to solving the weak formulation of elastodynamics equations keeps both, FEM geometrical flexibility and spectral methods accuracy.

To model different subdomains, such as structure and soil domains, and deal with complex 3D heterogeneous media, a discontinuous Galerkin (DG) approach is selected. The DG technique coupled with the SEM approach results in the DGSE method, which can connect materially and geometrically different (non-conforming) subdomains. The DGSE formulation deals, while keeping low computational effort, with non-uniform polynomial degree distribution and locally varying mesh size. Nevertheless, in this approach, every subdomain must be conforming.

The open-source numerical code SPectral Elements in Elastodynamics with Discontinuous Galerkin (SPEED), is used to evaluate the DSSI problem. This code performs parallel computing, in non-conforming grids, of seismic wave propagation in visco-elastic heterogeneous 3D media (Mazzieri, Stupazzini, Guidotti, & Smerzini, 2013). The DGSE approach implemented in SPEED allows to glue together different sub-domains (structure and soil) and model soil-structure effects, preserving efficiency and parallel processing speed.

2.2.3 Micro-vibrations analysis

Micro-vibration surveys were carried out using SARA® SL-06 triaxial seismographs. Experimental studies were performed at the sites and buildings. Every seismograph was installed over a tripod base with a bubble level, to ensure

instruments verticality. Each measurement was synchronized via GPS and was at least 30 minutes.

Using ambient vibration data from the building, the experimental dynamic properties of the structure are estimated. First frequencies and modal shapes are identified using Operational Modal Analysis (OMA) techniques. For this purpose, a simplified model is made using ARTeMIS® software of modal identification. Then, an optimization process was developed to calibrate the structural model to empirical modes.

On the other hand, the site's predominant period is estimated from geophysical measurements, which allows the estimation of the apparent impedance contrast between the layers of soil and the seismic basement. Later, a deep shear wave velocity (V_s) profile is estimated for both sites combining surface-wave techniques.

The flowchart shown in Figure 2-2 summarizes the general procedure.

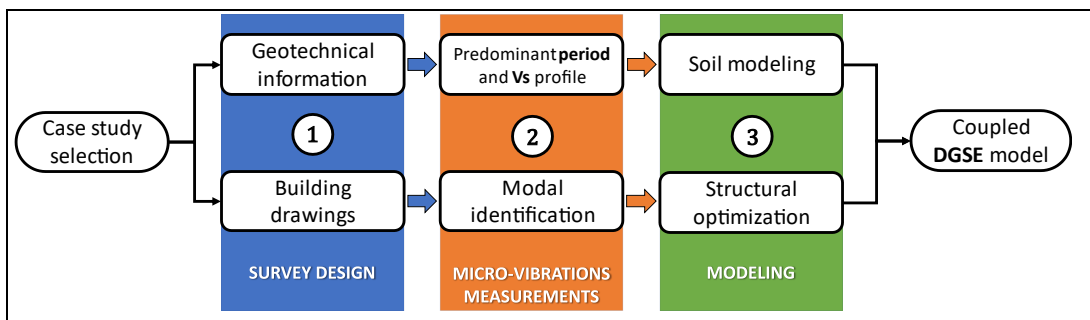


Figure 2-2: An overview of soil and structure modeling strategy.

2.3 Structure and soil modeling

2.3.1. Operational Modal Analysis (OMA) and modal optimization

The problem of system identification in vibrating structures relies on modal analysis, which separates complex vibration patterns into a set of modes of vibration. There are mainly two approaches to characterize the dynamic response of structures. First, the deterministic input-output (I/O) relation described by Experimental Modal Analysis (EMA). In this case, an artificial and measurable input is applied to the structure, the system output is measured, and the modal parameters are estimated through I/O spectrum division, to obtain the system frequency response function. The second approach is the stochastic framework used in Operational Modal Analysis (OMA), in the condition of a white noise input. This technique is applied in large structures, like buildings or bridges, subjected to non-measurable external excitations. Civil engineering structures are mainly loaded by ambient forces, so the stochastic process assumption is reasonably correct (Jacobsen, Andersen, & Brincker, 2007).

To obtain the structural response either all sensors are mounted once, or the sensors are moved in different configurations and multiple measurements are performed. Each configuration could be referred to as a *Test Setup*. In this study, multiple *Test Setups* measurement procedure are made. This procedure needs a couple of reference sensors, required to measure a good amplitude of all the mode shapes of interest, fixed in the same position in all the configurations (Structural Vibration

Solutions, 2019). Reference sensors were placed in the highest accessible floor in each building.

In the literature, several modal parameter estimation methods can be found. The most common techniques of modal parameters extraction are the Frequency Domain Decomposition (FDD) and the Stochastic Subspace Identification (SSI). The FDD method considers that modes can be estimated from calculation of spectral densities, under white noise and lightly damped structure conditions. Spectral density matrices are decomposed through the Singular Value Decomposition (SVD), which gives an estimation of the mode shapes (Gade, Møller, Herlufsen, & Konstantin-Hansen, 2005). In contrast, SSI method fits parametric models directly to the raw measured data. The parametric model is defined by a set of parameters, calibrated to minimize the deviation between the predicted system response and measured system response. Modal parameters are estimated from the SVD of the full observational matrix and extracting a subspace with the model modes (Herlufsen, Gade, & Møller, Identification Techniques for Operational Modal Analysis – An Overview and Practical Experiences., 2005). Among different algorithms of SSI techniques, the Principal Component (PC), Unweighted Principal Component (UPC) and Canonical Variate Analysis (CVA) are often used. Each one is a special case of user-defined weighting matrices that determine the state space basis. In the UPC algorithm, these weighting matrices are defined as identity matrices (Van Overschee & De Moor, 1996).

The FDD and SSI-UPC ARTeMIS® implementations of OMA are used for this study. The OMA performed in both buildings provides modal shapes and eigenfrequencies of each structure. Modal shapes are detected at equipment locations. Afterward, using linear kinematics, they are combined under the assumption of horizontal rigid diaphragm to complete the modal shape description of the building. The next step is to transfer this information into an elastic structural model, conformed only by volumetric elements, due to the selected modeling approach. Thus, the structural model is intended to balance its own complexity, be simple enough to run in available equipment and be complex enough to represent adequately the dynamical response. For this purpose, a modal optimization algorithm is developed. The algorithm is defined by an error quantification, computed from empirical and theoretical modal parameters, to be minimized. Matlab® optimization function *fmincon* is used to find the minimum of the multivariable error function, expressed as:

$$e = \sum_i^N \frac{1}{f_{ei}} \left(\alpha \frac{\|\boldsymbol{\Phi}_{ei} - \boldsymbol{\Phi}_{ti}\|}{\|\boldsymbol{\Phi}_{ei}\|} + \beta \frac{|f_{ei} - f_{ti}|}{f_{ei}} \right) \quad (2-1)$$

Where $\{f_{ei}, \boldsymbol{\Phi}_{ei}\}$ and $\{f_{ti}, \boldsymbol{\Phi}_{ti}\}$ are the empirical and theoretical frequencies and modal shapes respectively, α and β are scalar weighting parameters and N is the total number of modes used for the error computation. The term outside the parenthesis is meant to provide more relative importance to modes related to lower frequency eigenvalues. The minimization problem is subjected to linear constraints,

associated to the elastic modulus in order to ensure higher elastic modulus for lower stories:

$$\text{minimize } e \quad (2-2)$$

$$\text{subject to } E_j \geq E_{j+1} \quad \forall j = \{1..n - 1\}$$

Where E_j is the elastic modulus of the j -th set of walls and n is the number of different groups of walls. A wide range of β/α is explored to achieve the best adjustment possible, given the empirical data. For each building, the optimized model is identified to get the better representation both in frequency and modal shapes of the first two translational modes and, when possible, superior modes with a higher effective modal mass in the analyzed direction. As a result of the approach, the optimization algorithm exhibits a high dependency on the initial values. To overcome this bias, in each building, materials properties were manually adjusted to provide initial value closer to the empirical fundamental period (less than 1% of difference). With this calibration the algorithm improves greatly the adjustment of the vibration modes.

2.3.2. Geotechnical characterization

Based on a previous geophysical survey using surface-wave based techniques performed in Viña del Mar downtown (Podestá, Sáez, Yañez, & Leyton, 2019), initial material soil properties of the model are defined in terms of a non-linear relation between the depth (z), in meters, and shear wave velocity (V_s):

$$V_s(z) = 158.62 |z|^{0.2} \quad (m/s) \quad (2-3)$$

The horizontal to vertical spectral ratio (HVSr) technique or Nakamura method (Nakamura, 1989) is applied to estimate predominant frequency in the sites where studied buildings are located. Three simultaneous measurements of ambient vibrations for 180 minutes were performed using low frequency triaxial sensors. To process the measurements, the Stockwell Transform (S-Transform) is calculated in each component. Horizontal components are then geometrically combined to compute the horizontal to vertical ratio in the frequency domain accordingly with the methodology proposed by Leyton et al. (2012). Each measurement gives an estimation of the site's predominant frequency. Then, through interpolation, the value at the center of the building was estimated.

Once the site period is estimated, a soil column is made using Equation (2-3) for material properties, to estimate the local basin thickness. Iteratively, the depth is adjusted until its first elastic frequency matches the obtained site's predominant frequency. These values were verified against basin depth estimation made by gravimetry available in Soto et al. (2020). Because the building modifies the stress field due to its weight compared to excavated soil, Equation (2-3) was modified in terms of stress considering a uniform soil weight of $\gamma=1800 \text{ kg/m}^3$ accordingly to Podestá et al. (2019). Then, the soil confinement pressure is estimated directly with the building model, defined as the mean of the stress tensor trace. Finally, the vertical stress in each soil element is computed assuming a coefficient of lateral

earth pressure of 0.5, a typical value of granular soils. The adapted expression is presented, in terms of mean confinement pressure (p) and unit weight (γ):

$$V_s(p) = 172.02 \left(\frac{p}{\gamma} \right)^{0.2} \quad (m/s) \quad (2-4)$$

Additionally, in Soto et al. (2020), laboratory tests were performed to characterize cyclic inelastic soil behavior. In this work, a hyperbolic model was calibrated to provide shear modulus degrading and damping increasing curves as a function of the confinement. This model is used to represent the cyclic inelastic behavior of soils in the coupled model. Because the water table is shallow in this area, fully undrained curves were considered to account an eventual pore pressure increase during dynamic loading.

The non-linear soil behavior is assessed through the Linear Equivalent (LEQ) method, proposed firstly by Schnabel (1972) to solve a 1D wave propagation problem. This method considers nonlinearity using shear modulus degradation and damping curves, in terms of cyclic shear strain levels, in an iterative process. In the present study, this procedure is applied to update soil properties, after each iteration of the elastic coupled model subjected to the seismic input. For each run, the maximum shear strain is computed at the center of each soil element. Then, this value is reduced by the factor $R_\gamma = 0.65$ to estimate an effective shear strain (γ_{eff}). Because the model is 3D, the following equation is used for the evaluation of γ_{eff} , where ε_i are the eigenvalues of the strain tensor.

$$\gamma_{eff} = R_{\gamma} \max \{|\varepsilon_1 - \varepsilon_2|, |\varepsilon_1 - \varepsilon_3|, |\varepsilon_2 - \varepsilon_3|\} \quad (2-5)$$

The LEQ method is applied in each elastic iteration until convergence, defined by a maximum of 5% of difference in the shear modulus value in each element when compared to the previous iteration.

2.3.3. Seismic inputs

Here, the In Viña del Mar downtown there is only one seismic station that recorded both 1985 (Mw=8.0) and 2010 earthquakes (Mw=8.8), known as Viña Centro (VC) station in Figure 2-1. According to Podestá et al. (2019), sediment thickness in this location is about 30 m.

In order to simplify the interpretation of results and reduce the run time of the models, modified Ricker wavelets were used as seismic input, whose analytic equation is (Li, Dong, & Zhao, 2014):

$$R(t) = \frac{A}{f_1 - f_0} [f_1 \exp(-\pi^2 f_1^2 (t - t_0)^2) - f_0 \exp(-\pi^2 f_0^2 (t - t_0)^2)] \quad (2-6)$$

The main advantage of this synthetic ground motion is that, when compared to the standard Ricker wavelet, it exhibits a broader frequency band spectrum. Two signals were selected to cover different frequency ranges. The first input (R02-2) was chosen to cover the frequency range of available records at VC station, while the second (R05-5) was adjusted to cover the range of first empirical frequencies of both

buildings. The amplitude parameter (A) in Equation (2-6) was adjusted to match the Peak Ground Acceleration (PGA) recorded in available records at VC station. For this purpose, an iterative 1D soil column of 30 m depth is developed, then synthetic inputs and LEQ method are applied until the maximum acceleration at free field matches the reference PGA value. Results are shown in Figure 2-3.

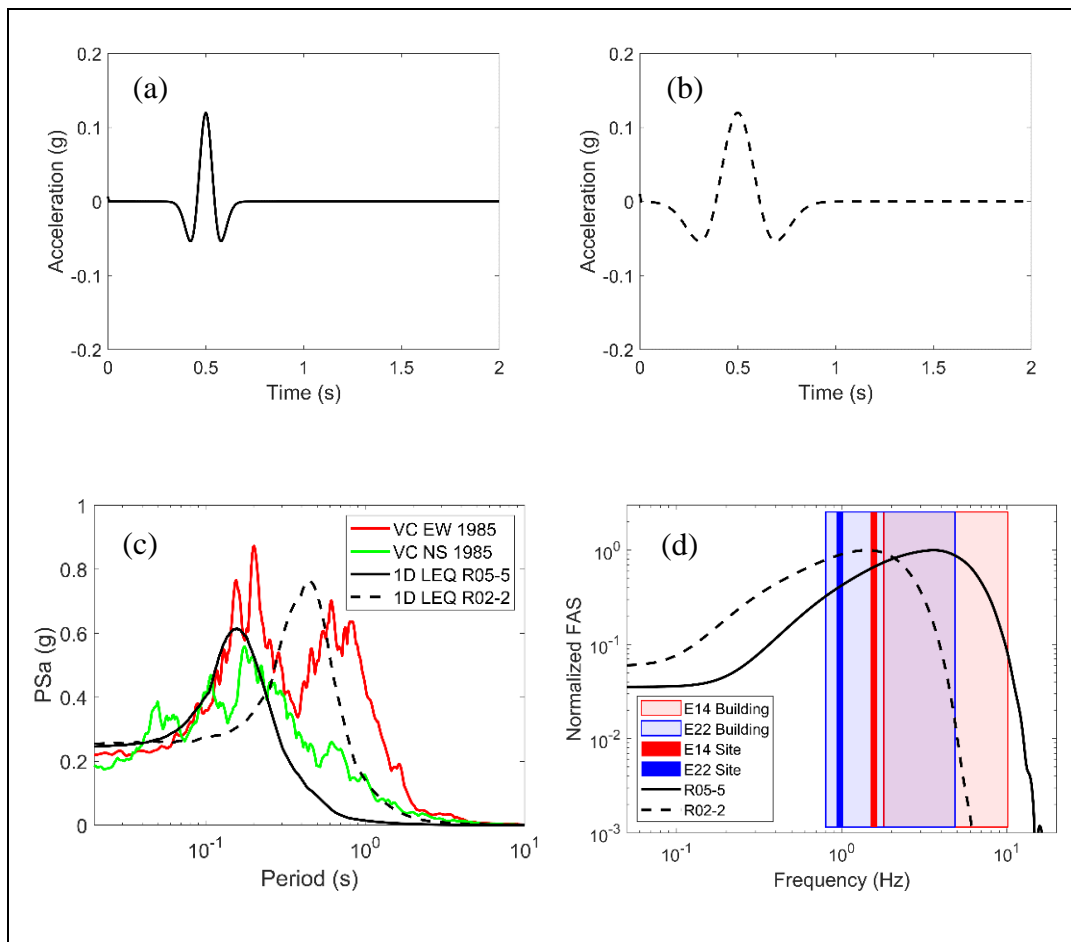


Figure 2-3: (a) R05-5 and (b) R02-2 Ricker wavelets. (c) Pseudo-spectral acceleration of synthetic motion and available records of 1985 Chilean Earthquake. (d) Normalized Fourier Amplitude Spectrum of the seismic inputs. Rectangles

indicate identified modal frequencies range of both buildings in red (E14) and blue (E22). Estimated predominant site's period is also shown.

2.4 14-story RC Building (E14)

2.4.1 Background

The first case study is a 14-story reinforced concrete building with one basement level, located in downtown Viña del Mar, approximately 200 m north from Marga Marga river and 700 m west of the shore. It also has a machine room in the top, of an approximate area of 1/5 the average story. The shear wall resisting system consists of a central corridor, one central elevator shaft, and four apartments per story, delimited by RC walls (see Figure 2-4). The stairs are in the center-south side of the floor plan. The typical story has 2.5 m height, while the basement and first story heights are 2.9 and 3 m respectively. The depth of foundation is about 3.4 m, including a 50 cm thick foundation slab. Typical floor dimensions are 17 m by 19 m. The basement level area is about 1200 m², L-shaped, and mainly dedicated to parking use. The building height above ground level is about 36 m and exhibits an aspect ratio (height to width) of 2.1 east-west in (*x*-axis) and 1.9 in north-south (*y*-axis) direction.

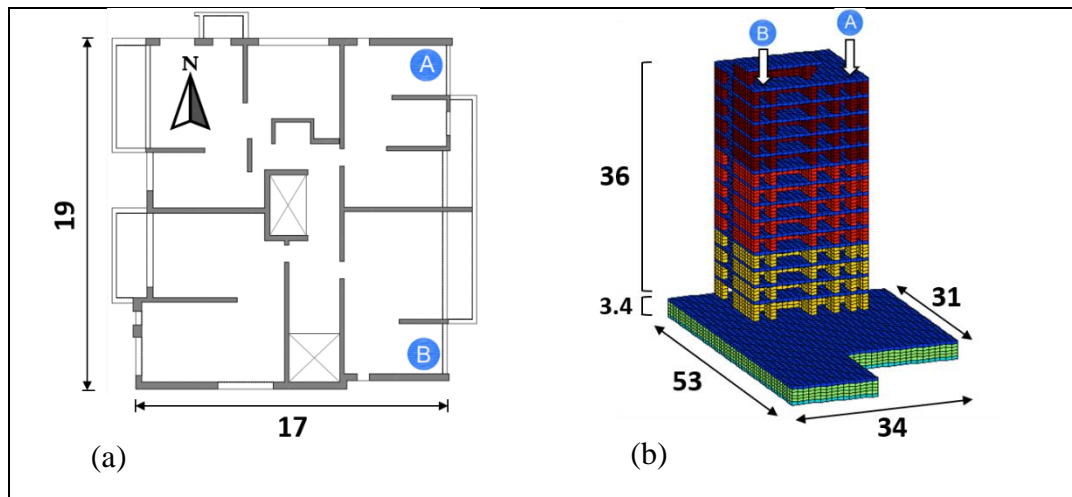


Figure 2-4: (a) Seismographs location on 2nd to 14th floor slabs. (b) Structural model. Dimensions are in meters.

2.4.2 Micro-vibrations analysis

The velocities Micro-vibration surveys were conducted using a 3D array of eight triaxial seismographs. The study consisted in installing four fixed reference sensors: the free field sensor (placed in a site next to the building), the base sensor (located in the basement slab) and two sensors placed on the 14th floor slab. The remaining four seismographs were installed in six different configurations. Each array considers two sensors per slab, starting from the 2nd floor to the 13th floor slab (12 levels total). Table 2-1 shows the instrument locations of each configuration. Later, in the simplified model developed in ARTeMIS® modal extractor, the first five frequencies and modal shapes are identified. These modes were determined using OMA-FDD and SSI-UPC methods. Modal identification results are shown in Figure 2-5b.

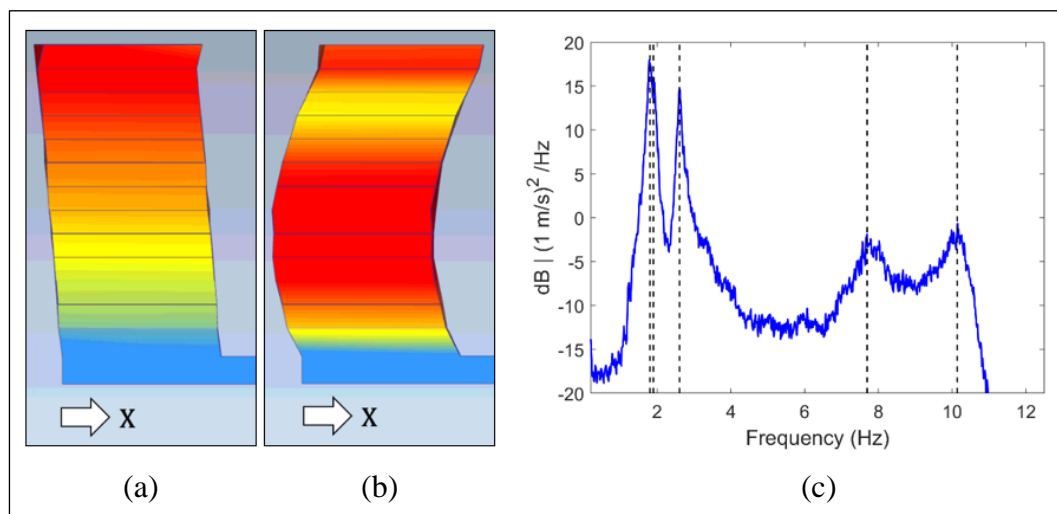


Figure 2-5: X-axis (EW) empirical modal shapes (a: $f = 1.8$ Hz, b: $f = 7.69$ Hz). Identified modal frequencies are shown in (c).

Table 2-1: Arrays summary. S-n indicates the instrument number, F.F. stands for free field, -1 is the basement level and N-A/B denomination refers to N-th floor slab, A or B location.

Array #	S-1	S-2	S-3	S-4	S-5	S-6	S-7	S-8
1	F.F.	-1	2-A	2-B	3-A	3-B	14-A	14-B
2	F.F.	-1	4-A	4-B	5-A	5-B	14-A	14-B
3	F.F.	-1	6-A	6-B	7-A	7-B	14-A	14-B
4	F.F.	-1	8-A	8-B	9-A	9-B	14-A	14-B
5	F.F.	-1	10-A	10-B	11-A	11-B	14-A	14-B
6	F.F.	-1	12-A	12-B	13-A	13-B	14-A	14-B

Three HVSR (Nakamura, 1989) measurements were performed to estimate the site's predominant period. A frequency of 1.57 Hz is interpolated at the center of the building from measurements close to the building. A basin depth of 49 m is computed for the site.

2.4.3 Coupled DGSE model

The structural model is calibrated using the proposed optimization process. After several trials, the number of different materials is reduced to six, representing for this building a better fit with a reduced number of parameters. The structural model intends to represent slabs and walls stiffness, using volumetric elements and aiming to keep the model as simple as possible. Two material properties are assigned to slab elements (building slabs and foundation slab), while four materials are designated to wall type elements. Every level preserves the same wall thickness for both principal directions but decreases in stiffness according to four groups of walls: 1) basement, 2) 1st to 4th level, 3) 5th to 9th level, and 4) 10th to 14th level. These groups were defined according to wall thickness decrease in the real building.

Slab mass density was adjusted to typical Chilean average unit weight per floor area of 10 kPa (Lagos, et al., 2012), stiffness properties were fixed stiff enough to ensure rigid diaphragm kinematics. Wall mass density was adjusted as the RC density (2.5 t/m³) times the ratio between the assumed shear wall density and the 6% average in Chilean RC buildings (Massone, et al., 2012). Once the slab properties are fixed, four parameters (wall elastic modulus as a proportion of slab value) were adjusted in the optimization procedure. The ratio between weighting factors in Equation (2-1) that exhibited the best fit was $\beta/\alpha = 1.92$. Initially calibrated model (M_{bef}) and optimized model (M_{opt}) results are shown in Figure 2-6 and Table 2-2. Modal participating mass ratios (N=20 modes) of M_{opt} in EW (U_x) and NS (U_y) directions are also presented below.

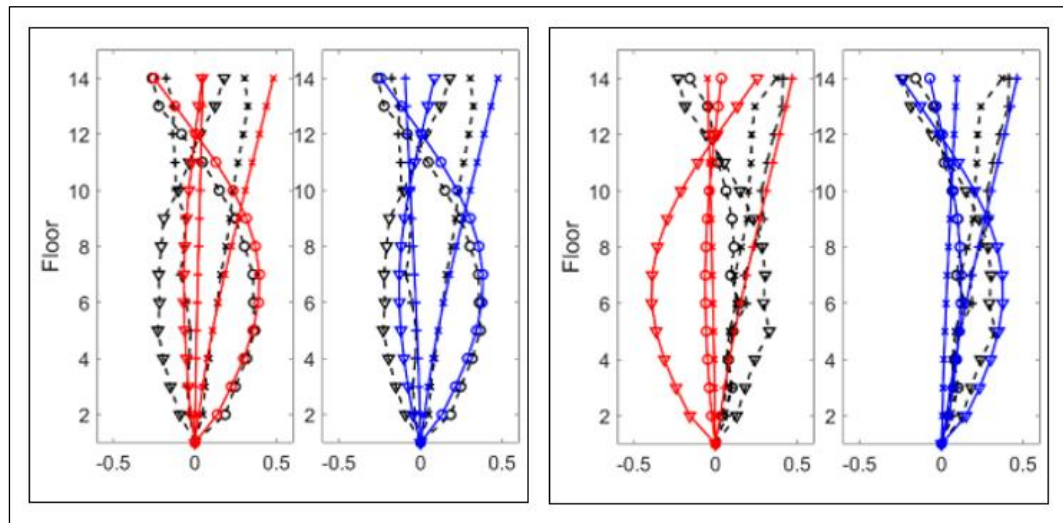


Figure 2-6: Empirical (black) and theoretical E14 modal shapes, prior (red) and after (blue) optimization (left: x -axis, right: y -axis). Markers: 1st (x), 2nd (+), 4th (o), and 5th (∇) mode.

Table 2-2 shows that before optimization natural frequencies were closer to target, but as can be seen in Figure 2-6, some modal shapes exhibited poor match with empirical data, especially in the y direction (NS). Modal participating ratios indicate that modeled modes are mostly uncoupled, being modes 1 and 4 activated in EW, modes 2 and 5 in NS, and mode 3 is mainly torsional. There is a reasonably good match in frequencies in first two natural frequencies (error below 8%). After optimization, in x -axis match is good (20-35% of difference) in relevant modes, while in y -axis very good (10-20% of difference) and good outputs are observed in mode 2 and 5, respectively. Satisfactory (35-50% of difference) to poor (>50% of

difference) results are only obtained in directions where the modes have below 1% of participating mass ratios, so this performance should not play a relevant role.

Table 2-2: E14 optimization results. Modal shape of the 3rd mode could not be properly estimated.

Mode	OMA (Hz)	M _{bef} (Hz)	M _{opt} (Hz)	U _x (%)	U _y (%)	Δf (%)	Δφ _x (%)	Δφ _y (%)
1	1.8	1.8	1.82	65.3	0.7	1.1	34.5	71.2
2	1.9	2.02	2.05	0.7	67.1	8.0	44.8	11
3	2.61*	3.9	3.18	0	0	22	-	-
4	7.69	7.12	6.74	21.3	0.6	-12.4	22.2	31.4
5	10.14	7.25	7.1	0.6	21.7	-30	46.4	23.7

To model the 49 m depth of the site, 12 layers of soil with variable height are defined. Elastic parameters of each layer were adjusted according to Equation (2-4). Below these layers, apparent bedrock elements are added. Before degradation, initial soil V_s vary from 175 to 336 m/s. Apparent bedrock properties were fixed at 2000 kg/m³ of density and $V_s=1200$ m/s. LEQ approach was applied only for soil layers. On the other hand, a damping factor of $\zeta = 5\%$ is assigned to the building and soil before degradation, while apparent bedrock is modeled with 1%. These properties are contained in the quality factors Q_s and Q_p , defined for the DGSE model as $Q_p = 1/\zeta$ and $Q_s = Q_p/2$.

Table 2-3: E14 DGSE model materials ranges.

Material	ρ (kg/m ³)	V_s (m/s)	V_p (m/s)	Q_s	Q_p
Building E14	625-2080	940-2200	1550-3630	10	20
Initial soil	1800	175-336	327-629	10	20
Bedrock	2000	1200	2245	50	100

The DGSE model consists of a non-conforming mesh of 4 subdomains: building, fine mesh soil (neighboring to the building), coarse mesh soil, and bedrock. The model has a total of 37644 linear nodes, 20973 hexahedral, and 5321 quadrilateral elements. From those, 16017 hexahedral elements correspond to the building, while 4956 are soil and bedrock elements. Because of the selected SEM approach, this model has 1631906 spectral nodes.

In order to glue structural (mesh size of $h = 0.5\text{--}0.86\text{ m}$) and soil subdomains, a DG surface is created, covering the soil-structure boundary. Two more DG surfaces are included to connect coarse mesh soil ($h \sim 6\text{ m}$) with the fine mesh close to the building ($h \sim 3\text{ m}$) and the bedrock below ($h \sim 12\text{ m}$). Figure 2-7 shows the mesh distribution in the 3D model.

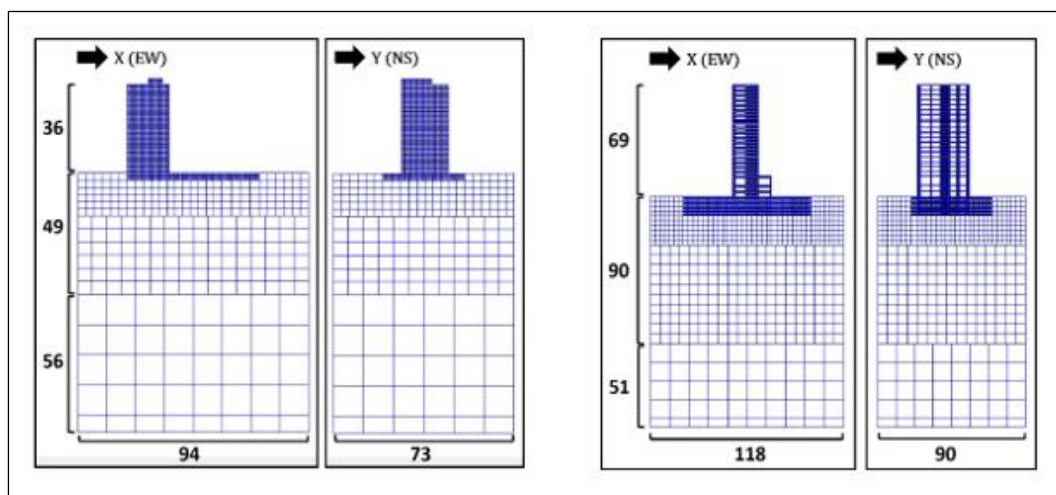


Figure 2-7: Coupled 3D model. Dimensions are in meters (left: E14, right: E22).

2.5 22-story RC Building (E22)

2.5.1 Background

The second case study is a 22-story reinforced concrete building with four parking levels (see Figure 2-8). Its location is approximately 600 m. north from Marga Marga river and 800 m. west of the shore. The building was constructed with a 10 cm seismic joint, which dynamically separates the structure behavior in two substructures: the core building (the tower) and the surrounding structure below ground level (the parking building). The tower floor dimensions are 24 m by 32 m (4th basement to 3rd floor) and 16 m by 32 m (4th floor to 22nd floor). The parking building area is about 2600 m².

Despite its heterogeneity, the resisting system can be defined as an RC core wall plus exterior columns. In lower stories (4th basement to 3rd floor), exterior columns are on both sides (east and west) of the floor, besides a core shear wall system. However, in 4th to 22nd level portion, only west side columns continue to the roof, while the shear walls constitute the east side of the floor. RC walls contain two central elevator shafts and two stairs (on the north and south sides).

The typical story has 3 m height and the basement levels are 2.6 m. Exceptions are the first basement (3.1 m), first to third stories (3.6, 3.4 and 5.5 m), and a technical story (1.75 m). The depth of foundation is about 11.8 m, including a 90 cm (tower) or 60 cm (parking building) thick foundation slab. The building height above ground level is about 69 m and exhibits an aspect ratio (height to width) in the typical story

of 4.3 in east-west (x -axis) and 2.1 in north-south (y -axis) direction, making it a medium slender structure in the x -direction.

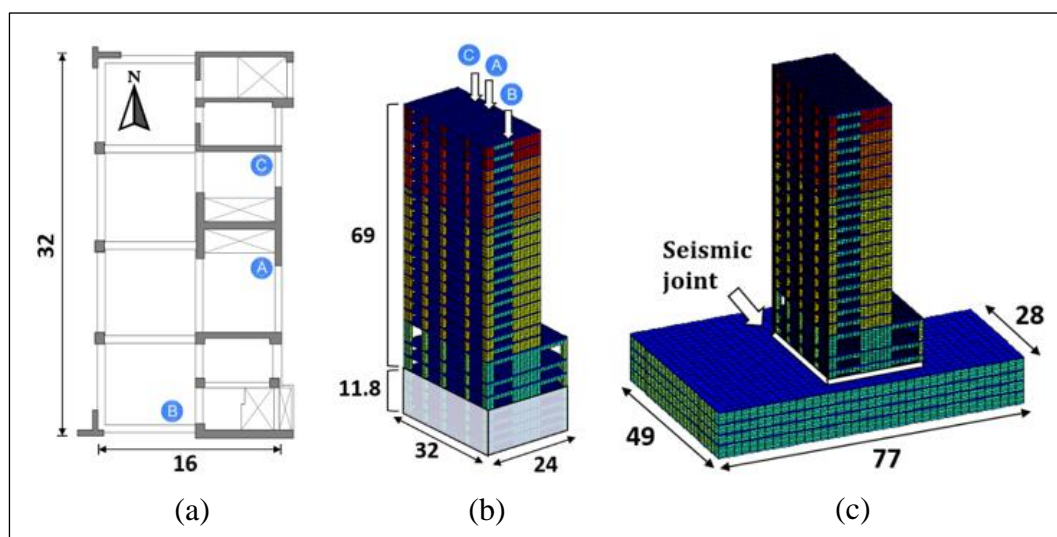


Figure 2-8: (a) Seismographs location on 2nd to 20th floor slabs. (b) Tower and (c) Structural model including the parking building. Dimensions are in meters.

2.5.2 Micro-vibrations analysis

Micro-vibration surveys were conducted using a 3D array of seven triaxial seismographs. The study consisted in locating four fixed reference sensors: the free field sensor, the base sensor (located in the 4th basement slab), and two sensors placed on the 20th floor slab. The remaining three seismographs were installed in six different configurations. Table 2-4 displays the instrument locations of each configuration. In ARTeMIS® modal extractor, first seven frequencies and five modal shapes are detected. These modes were determined using OMA-FDD and SSI-UPC methods. Modal identification results are shown in Figure 2-9.

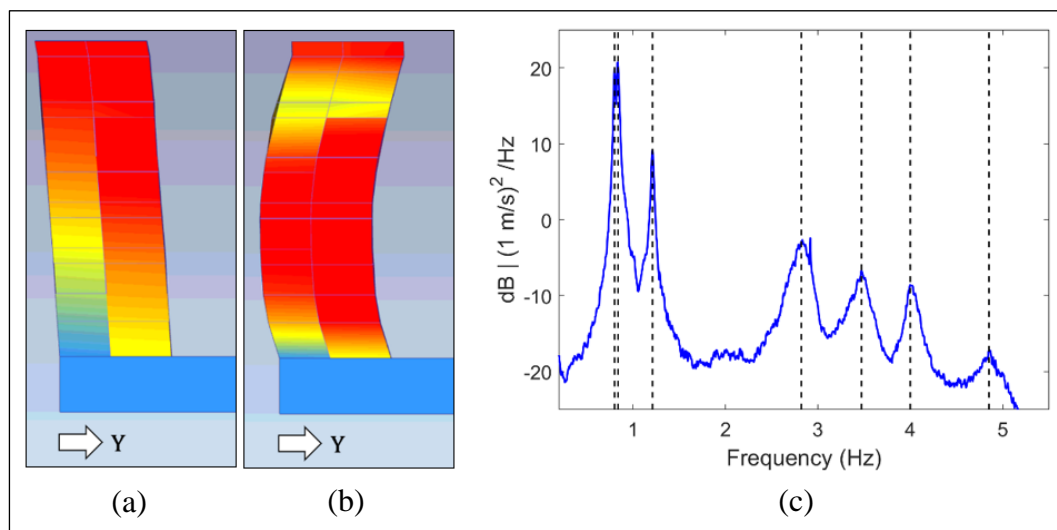


Figure 2-9: Y-axis (NS) empirical modal shapes (a: $f = 0.8$ Hz, b: $f = 2.82$ Hz). Identified modal frequencies are shown in (c).

Table 2-4: Arrays summary. S-*n* indicates the instrument number, F.F. stands for free field, -4 is the 4th basement and N-A/B/C denomination refers to N-th floor slab, A, B, or C location.

Array #	S-1	S-2	S-3	S-4	S-5	S-6	S-7
1	F.F.	-4	19-C	18-B	18-C	20-C	20-B
2	F.F.	-4	16-C	15-B	15-C	20-C	20-B
3	F.F.	-4	4-A	12-B	12-A	20-C	20-B
4	F.F.	-4	13-A	9-B	9-A	20-C	20-B
5	F.F.	-4	10-A	6-B	6-A	20-C	20-B
6	F.F.	-4	7-A	3-B	3-A	20-C	20-B

Based on the application of the HVSR method, a frequency of 0.98 Hz was adopted to the building. A basin depth of 90 m is computed for the site.

2.5.3 Coupled DGSE model

The structural model is calibrated using the same procedure for E14. In this case, 14 materials are defined. Two material properties are assigned to slab elements (building slabs and foundation slab), while 12 materials are designated to wall type elements. Each level has two principal directions stiffness and decreases in height according to five groups of walls: 1) basements, 2) 1st to 3rd level, 3) 4th to 15th level, 4) 16th to 20th level, and 5) 21st-22nd level. The remaining two materials were assigned to parking building walls. The optimization is made only over the tower, due to the seismic joint.

Slab and wall mass density was adjusted as similar as E14. Ten parameters were calibrated in the optimization procedure. The ratio between weighting factors in Equation (2-1) that exhibited the best fit was $\beta/\alpha = 2.75$. The calibrated model and its results are shown in Figure 2-10 and Table 2-5. Compared to E14, identical criteria were adopted to build 3D soil-building model. Model properties are summarized in Table 2-6.

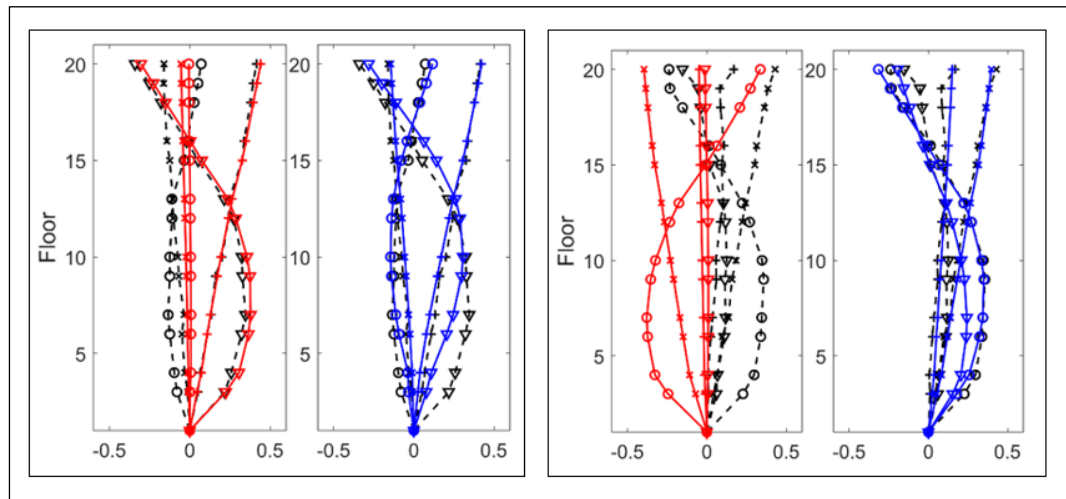


Figure 2-10: Empirical (black) and theoretical E22 modal shapes, prior (red) and after (blue) optimization (left: x -axis, right: y -axis). Markers: 1st (x), 2nd (+), 4th (o), and 5th (∇) mode.

Table 2-5 shows that modal results in E22 are significantly more coupled than E14, especially in higher modes. Modes 1 and 4 are mostly NS, mode 2 is EW, and mode 3 is lateral-torsional. Regarding frequencies match against empirical data, the optimized model performs remarkably good (error below 14% in all modes). Indeed, first two modes have an excellent performance (<10% of difference) in their relevant directions. In x -axis, results are excellent to good (<20%) in all modes (except mode 7), while in y -axis good (20-35%) and very good (10-20%) outputs are observed in modes 2 and 4 respectively. Poor performance of relevance is reported only in mode 5 (NS), which has about 6% of participating mass ratio in this direction. Mode 7 was not considered in the optimization process since it has a very low contribution in total structural response.

Table 2-5: E22 optimization results. Modal shapes of (*) frequencies could not be estimated.

Mode	OMA (Hz)	M_{bef} (Hz)	M_{opt} (Hz)	U_x (%)	U_y (%)	Δf (%)	$ \Delta\phi_x $ (%)	$ \Delta\phi_y $ (%)
1	0.8	0.8	0.82	5.7	58.1	1.7	20.1	7.6
2	0.84	0.84	0.87	51.8	9.7	4.3	7.7	35.7
3	1.21*	1.21	1.16	6.3	2.7	-4.2	-	-
4	2.82	2.7	2.55	1.9	10.1	-9.5	35.6	11.4
5	3.47	3.28	3.00	8.2	5.8	-13.3	32.7	93.4
6	4.00*	3.84	3.77	7.6	1.3	-5.8	-	-
7	4.85	5.32	4.9	1.6	0.2	1.0	72.3	85.9

Table 2-6: E22 DGSE model materials.

Material	ρ (kg/m ³)	V_s (m/s)	V_p (m/s)	Q_s	Q_p
Building E22	674-2500	241-3402	397-5612	10	20
Initial soil	1800	171-387	320-724	10	20
Bedrock	2000	1200	2245	50	100

This DGSE model also consists of a non-conforming grid of 4 subdomains: E22 building, neighboring fine mesh soil, coarse mesh soil, and apparent bedrock. The model has a total of 124536 linear nodes, 67419 hexahedral, and 10200 quadrilateral elements. From those, 53191 hexahedral elements correspond to the building, while 14228 are soil and bedrock elements. This model has 5219172 spectral nodes.

Structural (mesh size of $h=0.5-1$ m) and soil subdomains are also glued by a DG surface in the soil-structure boundary. Besides, two more DG surfaces are defined to connect coarse mesh soil ($h \sim 6$ m) with the fine mesh soil above ($h \sim 3$ m) and the bedrock below ($h \sim 12$ m). Vertical planes between the tower and parking

buildings are independent, i.e. relative displacement between both buildings can simulate seismic joint (see Figure 2-8c).

2.6 Results

A traditional way for the estimation of the DSSI effects is through a structure-to-soil stiffness parameter (Veletsos & Nair, 1975; Bielak, 1974) defined as the ratio between the building height \mathbf{h} to fundamental period \mathbf{T} relation (representing structural stiffness) and an average effective shear velocity of the site ($\mathbf{V}_{s\text{-avg}}$), computed as $(\mathbf{h}/\mathbf{T})/\mathbf{V}_{s\text{-avg}}$. The general procedure of this computation is detailed in NEHRP (2012), where the effective profile velocity is calculated using vertical translation and rocking vibration modes of the foundation. On the other hand, Chilean seismic code NCh433 (2009) and D.S. 61 (2011) classifies both sites as soil type D, based on the average V_s computed over first 30 meters depth (\mathbf{V}_{s30}). Then, assuming \mathbf{V}_{s30} as the effective shear wave profile, the structure-to-soil stiffness ratio is 0.18 (E14) and 0.17 (E22). Therefore, as these values are significantly higher than 0.1, important inertial SSI effects would be expected for both buildings (Stewart, Seed, & Fenves, 1999), such as period lengthening and foundation damping.

Three modeling approaches were considered: A fully coupled 3D model (S3D) and two uncoupled models (see

Figure 2-11). The uncoupled model approach consists of isolating the structure from the S3D model and apply two boundary conditions: fixed at the base (M1) and full fixation of the embedded portion (M2), assuming infinite stiffness of the adjacent soil. In current Chilean design, lateral soil is neglected, considering fixed lateral

displacements and vertical springs at the base (M1 condition is equivalent to infinite rigid springs). In the case of M2 assumptions, common shear wall buildings in Chile are characterized by below-grade perimeter walls that are thick enough to assume a stiff-box behavior in the underground portion, so that no significant drift demands are expected (Lagos, et al., 2012).

Embedment effect over the seismic forces is assessed via an input calibration. A 1D column of soil (S1D) is developed using DGSE and LEQ approach, at each site. From S1D two seismic inputs are extracted: a foundation input motion (FIM, at the foundation depth) and a free field motion (FF, at column's grade level). Thus, the combination of applying two inputs over two boundary conditions, while preserving the structural model, in two directions (EW and NS), provides comparison framework between coupled models and current seismic building design. Effects over ground motion, soil, and structural seismic demands are presented and compared below.

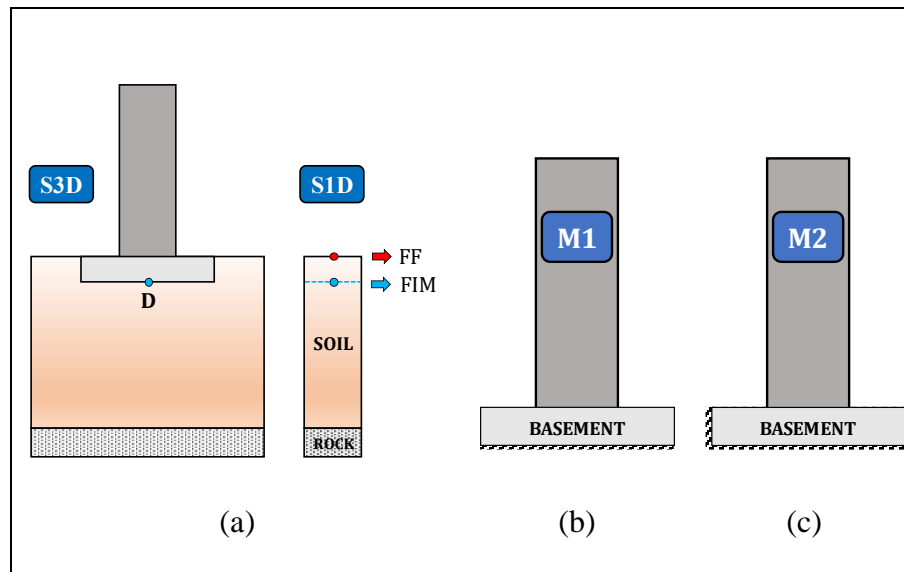


Figure 2-11: (a) Coupled 3D Model (S3D) and column of soil (S1D). Free field (FF) and foundation input motions (FIM) are extracted and applied over uncoupled structures models M1 (b) and M2 (c).

2.6.1 Ground Motion and soil

This section addresses the modification of ground motion in the presence of a building. This is evaluated in terms of PGA at free surface, pseudo-spectral acceleration (PSa) and profiles of soil maximum acceleration, and effective shear strain. All the comparisons are made over the last iteration of S3D and S1D models of the LEQ approach.

In general, building-induced effects are negligible in soil below 25 meters depth. Three points (**A**, **B**, and **C**) have been chosen (Figs. Figure 2-12 and Figure 2-13) to analyze both superficial and in depth effects. In all cases, the vicinity of the buildings

exhibits lower accelerations, associated with the soil-building boundary and an increase of lateral stiffness. Nevertheless, points outside the building's vibration (or loading) direction reaches approximate free field condition compared to S1D results. This is especially evident for R02-2 lower frequency input, where effects over the soil tend to present smoother transitions than R05-5, which presents peak zones caused probably by short wavelength reflections (for instance, point **B**). Indeed, in this case short wavelength associated to higher frequency content is more comparable to the basement size (i.e. seen as wave obstacle).

Soil columns below points **A**, **B**, **C**, and **D** (base of buildings) are shown in Figs. Figure 2-14 and Figure 2-15 in terms of soil acceleration and maximum effective shear strain in upper 30m. Comparing S1D and S3D, both sites exhibit lower differences in the response when subjected to the lower frequency seismic input. Differences in E14 site response to R02-2 may be neglected in soil deeper than the building base. Under the same loading, E22 site shear strain results are similar between S1D and S3D cases, but S3D presents up to 20% increase in acceleration peak response. Besides, analyzing the effects of the base slab, E14 site presents lower soil shear strains above the base level, as the building elements are stiffer than the surrounding soil, the soil is unloaded while the structure takes part of the horizontal seismic forces. However, in E22 site, the effects of basements are more erratic, since acceleration peaks increase in S3D cases, but soil strains do not exhibit a clear tendency. Even so, the larger peaks increase under R05-5 suggest that these results may be related to short wavelength superposition because maximum acceleration is

a parameter related to the higher frequency content of the motion, while keeping strains comparable to SID response.

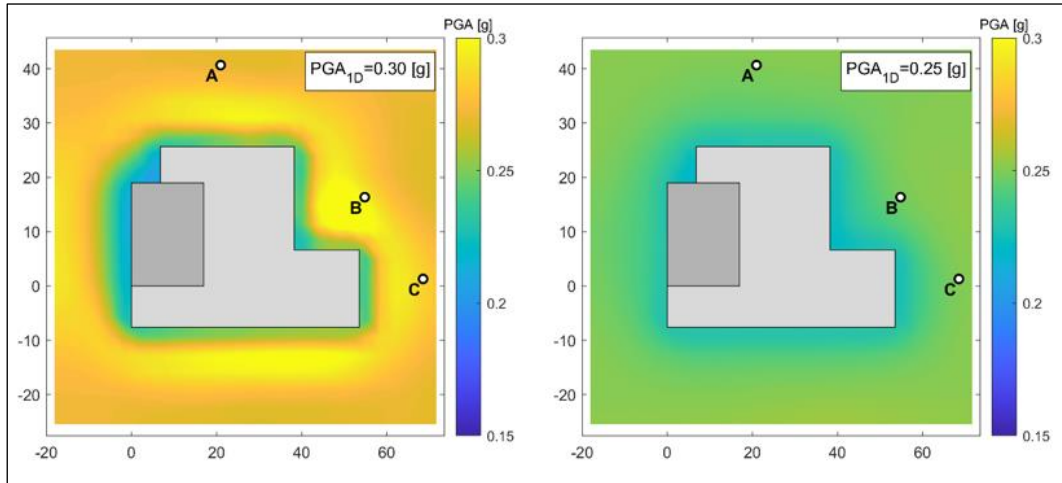


Figure 2-12: Free field PGA of E14 loaded in x -axis (left: R05-5, right: R02-2).

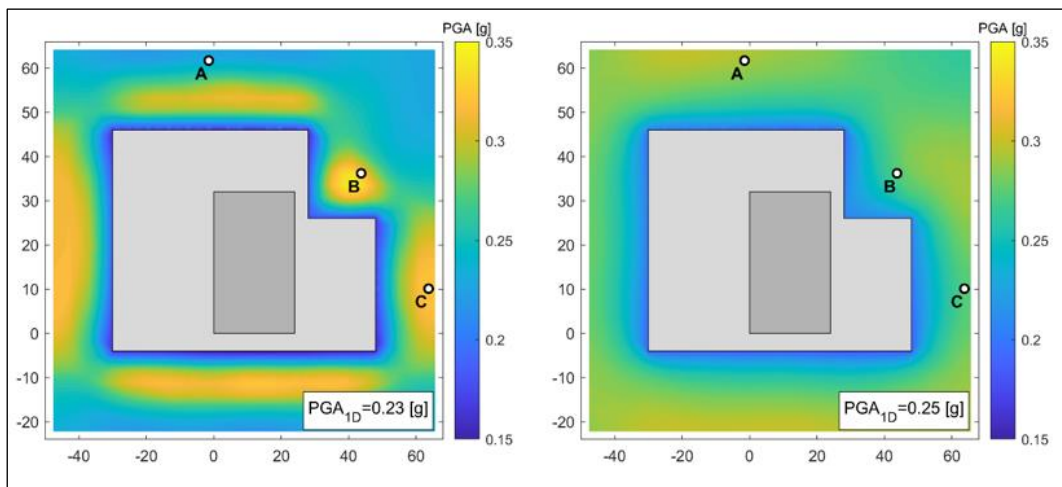


Figure 2-13: Free field PGA of E22 loaded in x -axis (left: R05-5, right: R02-2).

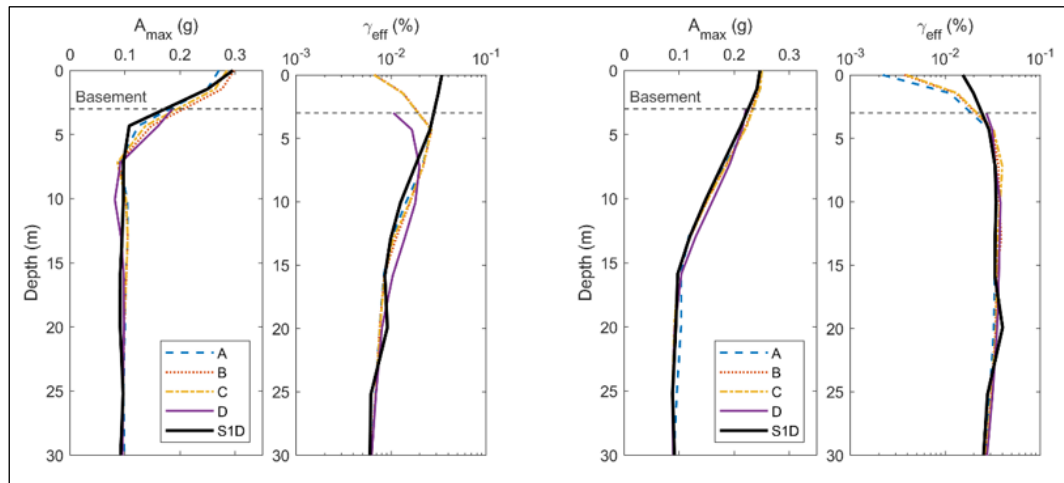


Figure 2-14: Columns of E14-S3D vs. S1D in x -axis (left: R05-5, right: R02-2).

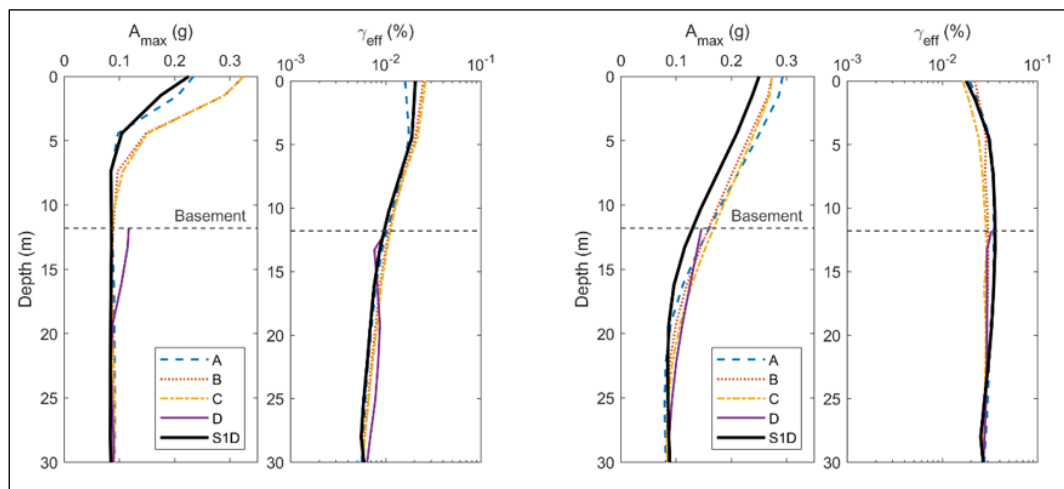


Figure 2-15: Columns of E22-S3D vs. S1D in x -axis (left: R05-5, right: R02-2).

The pseudo-acceleration analysis indicates that the spectrum peak response is clearly controlled by the input predominant frequency. As may be seen in Figure 2-16, building effects over the base (point **D**) ground motion are low to moderate. In the case of the motion at free surface (point **B**), even considering its proximity to the

structure (around 15 m), all results show minor differences, except E22 site response to R05-5. This case is directly related to the substantial local increase of PGA at surface in S3D model reported above. Besides, elastic soil periods in E22 site (both inputs) and E14 subjected to R05-5 are not associated with clear peaks. However, E14 site response to R02-2 shows a second spectrum peak that matches the elastic predominant period of soil.

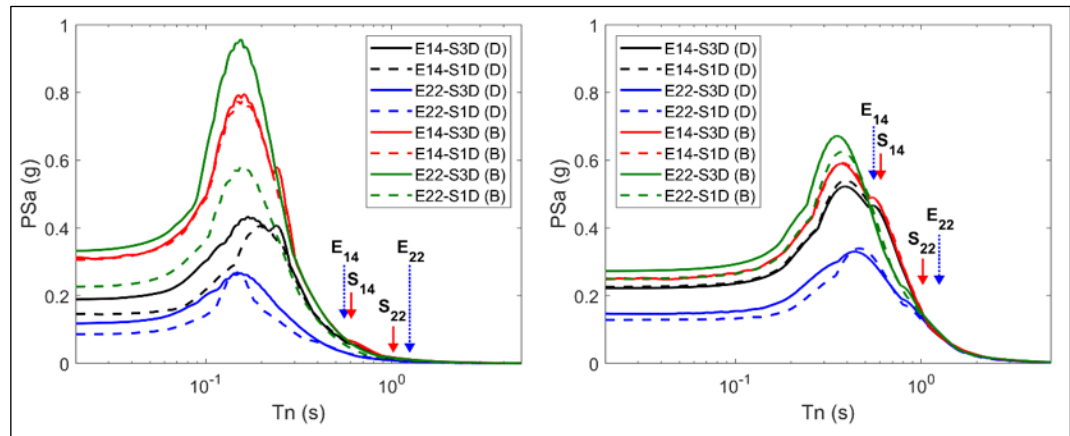


Figure 2-16: Pseudo-spectral acceleration of building base (point **D**) and free surface motions (point **B**), loaded in x -axis (left: R05-5, right: R02-2). Predominant elastic soil (S_{14} and S_{22}) and fixed base building (E_{14} and E_{22}) periods are also shown.

2.6.2 Structural response

Several simulations have been performed over the combination of two buildings, sites, ground motions, directions, and fixity conditions. Figure 2-17 shows the spectral ratio results between the signal recorded at the roof and the building base (point **D**) level. In these graphs, ambient noise amplitude is normalized to M1 output.

Firstly, in E14 building fixed base models M1 ($f = 1.82$ Hz) and M2 ($f = 1.86$ Hz) reasonably match the ambient data peak ($f = 1.79$ Hz). Indeed, the models were calibrated based on OMA, that gave slightly different values to ambient noise spectral ratio. Meanwhile, in E22, M1 model peak ($f = 0.82$ Hz) present a slight variation from ambient ($f = 0.8$ Hz), while M2 exhibit an increase of 16% ($f = 0.93$ Hz). This difference is explained by the M2 fixation of E22 building where the seismic joint is fully fixed against displacements, since the M2 approach firstly applied in E14 has no meaning in this case.

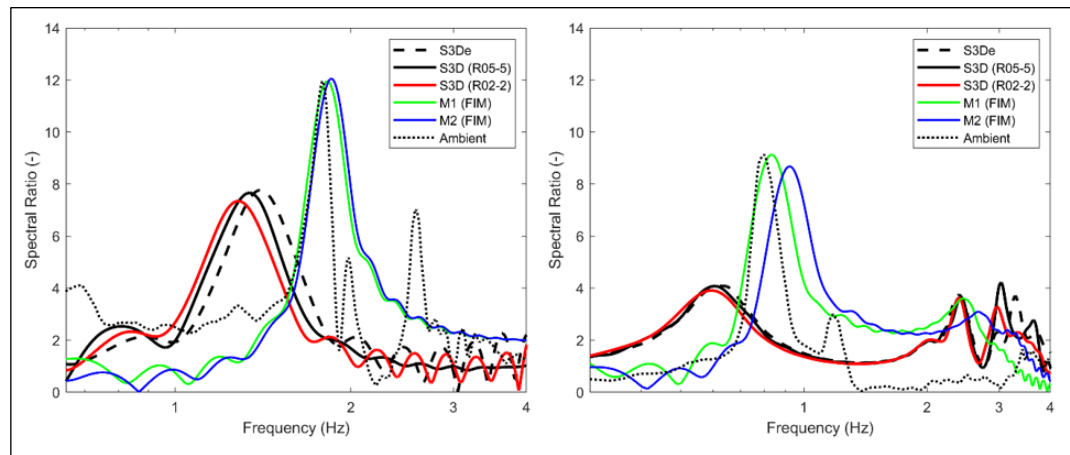


Figure 2-17: Spectral Ratio between building top and base. Initial elastic model (S3De) is compared against S3D LEQ and uncoupled models (left: E14 EW, right: E22 NS).

Regarding S3D results, Figure 2-17a points out a significant period lengthening of almost 30% in the DSSI elastic output, while LEQ cases reach an increase up to 36% (R05-5) and 42% (R02-2), all of them compared to M1 elastic uncoupled runs in EW

direction. Furthermore, Figure 2-17b indicates a period lengthening of 28% (DSSI elastic run) and LEQ cases increase about 34% (R05-5) and 37% (R02-2). Finally, the amplitude decreases in all DSSI cases: E14 exhibits a reduction of 35-39% and E22 decrease by 50-53%. This phenomenon might be associated with important radiation and material damping effects.

Interstory drifts and story shear comparisons are presented below. Results in both structural main directions, EW and NS, were obtained loading in x -axis and y -axis, respectively. Computation of interstory drifts in S3D are assessed in two ways: 1) simply as the difference in lateral displacements between consecutive stories normalized by the story height, and 2) also considering a correction, defined as S3D (FR), subtracting an estimation of the lateral displacements induced by base slab rocking (assumed as rigid body rotation of the building).

Based on the results shown in Figure 2-18 and the presence of a seismic joint in E22, the computation of the drift correction is done using the floor dimensions of the tower in both cases (i.e. 17 m by 19 m in E14 and 24m by 32 m in E22). Being the case that the rest of the base slab, dedicated to parking spaces, behaves nearly independent from the portion of the building base projected by the superstructure above ground level.

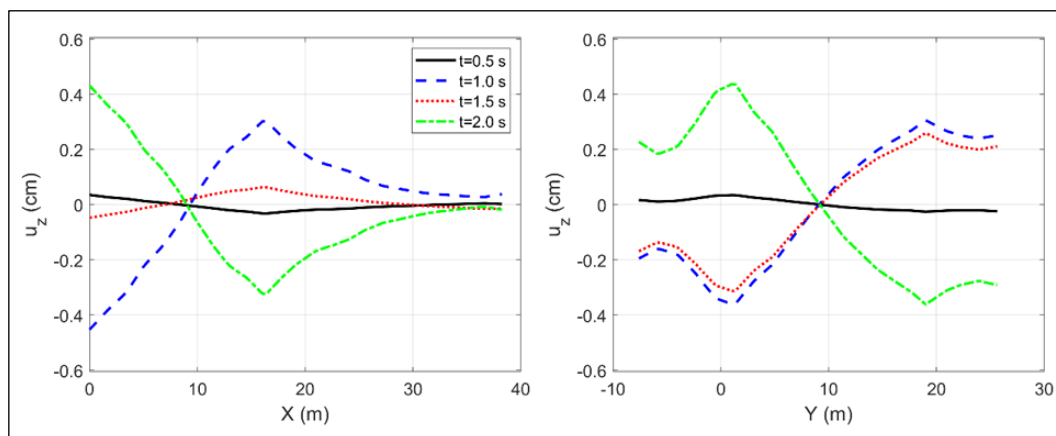


Figure 2-18: Vertical displacements snapshots of E14 building base slab under R02-2 action (a: EW, b: NS). Tower typical floor dimensions are 17 m (EW) by 19 m (NS).

Figure 2-19 shows that E14 drifts below 10.6 m height (5th floor slab) are always higher in S3D simulations, and that differences between M1 and M2 approaches are negligible, being the case that E14 has only one subterranean level. Besides, regarding R02-2 ground motion, FF and FIM do not show significant differences in their peak amplitude (about 10%). In contrast, R05-5 observed peak in FF is about twice the FIM amplitude.

Under the action of R05-5 input, E14 drifts in both components exhibit small differences with FF (below 5th floor) and FIM (above 5th floor) outputs. Roof drift increases up to 50% under FF motion in NS component. On the other hand, when subjected to R02-2, in x -axis, floors located in the upper half seem unaffected by the modeling approach. In y -axis, S3D response is higher than uncoupled models. In this case, compared to EW, NS roof response decreases by 10-14% in S3D, while M1

and M2 experience a decrease of almost 25%, probably based on a lower modal contribution of superior modes in this direction. Table 2-2 shows that optimized 5th mode (mainly y-axis) has a frequency that may be modestly excited by the lower frequency motion. However, DSSI gives rise to lower and more closely natural frequencies, so it is reasonable to expect that S3D response can be amplified by this input.

If the drift correction is considered, R05-5 induces an intermediate response in lower levels (below 4th story) in S3D. However, stronger effects are observed in R02-2 drift correction, lowering the raw interstory drift by 40-42%. Thus, S3D (FR) exhibits notably lower drifts than uncoupled cases, with a decrease in the roof response of about 34% (EW) and 31% (NS) when compared to M1 subjected to FF motion.

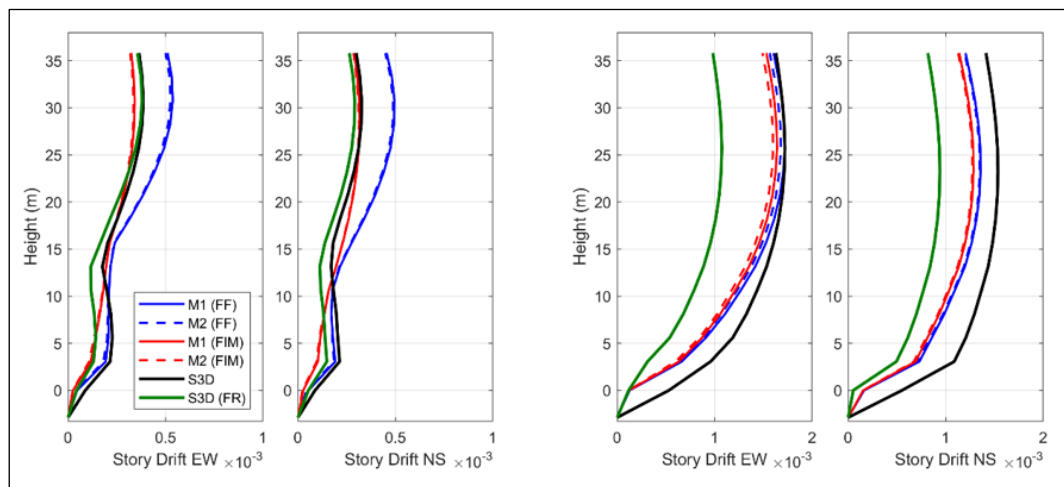


Figure 2-19: E14 Interstory drifts (left: R05-5, right: R02-2).

Story shear envelope is computed using D'Alembert's Principle based on inertial forces. This term is calculated using absolute story accelerations. Figure 2-20 shows

story shear distribution in E14. In the higher frequency input, FIM and FF are, except for a few stories, lower-bound and upper-bound curves, respectively. Computed base shear is about 27% lower in FIM case, while FF input induces an increase of about 40-47%, in comparison to S3D structural response. Due to R02-2 action, it was observed that S3D shear response is remarkably lower than all uncoupled cases. S3D approach presents a significant reduction in both directions, i.e. uncoupled models exhibit an increase of 125-136% (EW) and 75-86% (NS) in their relative base shear results. E14 shear trend is the opposite of the one observed in relative displacements because this model presents lower peaks of absolute acceleration, then the story shear envelope is also lower than uncoupled models. Apparent discrepancy between the observed trend in terms of displacement and shear force (accelerations) for R02-2 input might be related to the relative flexibility of the foundation slab. Indeed, although it is a 50 cm thick concrete slab, it has a length of more than 30 m (or 50 m) depending on the load direction, hence it is unlikely that it will behave as a rigid element under long wavelength seismic loading. Then, the rocking motion includes some bending of the foundation slab, as can be seen in Figure 2-18. Therefore, once the drift is corrected by the rocking of the base slab portion below the tower, interstory drift and story shear envelope do follow the same trend.

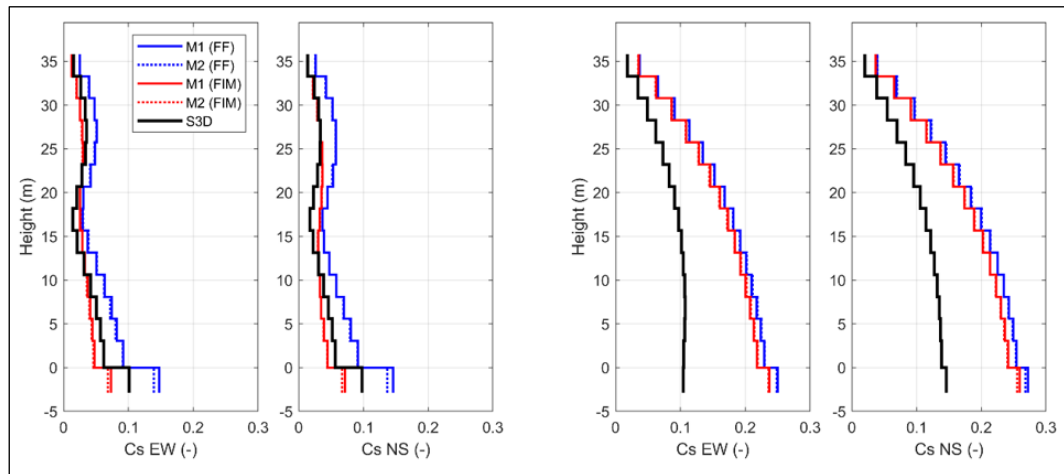


Figure 2-20: E14 Story shear coefficient (left: R05-5, right: R02-2).

Figure 2-21 shows interstory drifts of E22. Because of M2 approach, subterranean levels exhibit near zero displacements. When E22 is subjected to R05-5, FIM and FF over M1 are lower-bound and upper-bound curves respectively, in both directions. M2 also exhibits the same trend, but above the 2nd floor due to the embedded portion of the structure. In the case of R02-2, in EW direction is observed that below 4th floor slab S3D response is larger than uncoupled cases, while this behavior is reported only in basement levels in the other direction. In 4th to 15th levels, S3D drifts are notably lower than M1 and M2, this response matches an important reduction of both stiffness and story dimensions (24 m to 16 m in EW size). Above these floors, S3D has a material stiffness reduction and tends to follow FIM curves. Regarding S3D (FR), base rotation correction has a minor effect in the overall trend for the R05-5 input, but in R02-2 (longer wavelength) the tendency of larger drifts in lower stories is reversed. However, this correction is an estimation of the effects of rigid body

rotation, maximum interstory drifts are probably somewhere in between black and green curves in Figure 2-21. Because the seismic joint, the effective mat foundation considered to estimate rigid body rotation is only the base slab below the tower, neglecting effects of the parking building. Indeed, according to available information, the foundation slab under the building is significantly thicker than in the parking area, so that they are approximately independent.

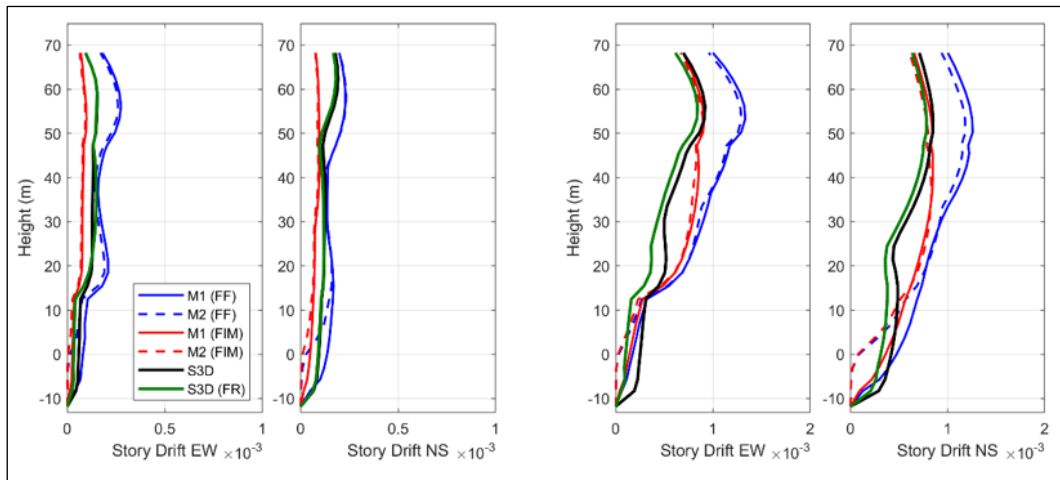


Figure 2-21: E22 Interstory drifts (left: R05-5, right: R02-2).

Story shear forces follow the same behavior reported in M1 drifts under R05-5 action,

as can be seen in

Figure 2-22. Thus, FIM causes a moderate change (EW: 15% higher and NS: 22%

lower), while FF response is augmented up to 180-220% compared to S3D base

shear. In the case of R02-2, S3D exhibits an envelope of forces lower than observed

in FIM and FF, although its shape is more like FF. Under FIM, base shear increases

up to 25%, while FF induces a response roughly twice in magnitude in both directions (

Figure 2-22).

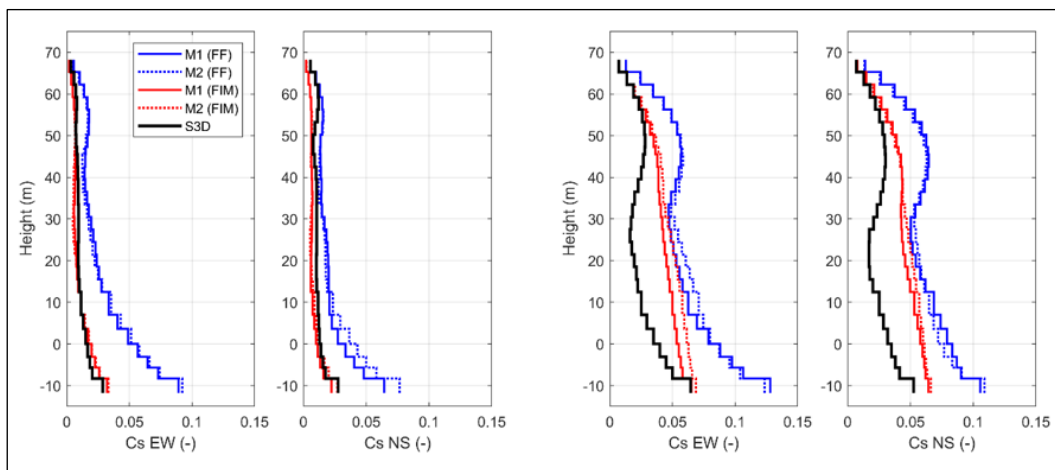


Figure 2-22: E22 Story shear coefficient (left: R05-5, right: R02-2).

2.7 Conclusions

The scope of the investigation was to propose a methodology to quantify DSSI effects in buildings with underground levels, evaluate soil non-linearity impact over the structural response, and to compare different approaches to model soil-structure interaction in shear wall buildings on medium stiff sandy deposits. A 3D model for seismic wave propagation was developed for each real building located in Viña del Mar city. The novelty of this study is to use ambient micro-vibrations to calibrate not only the soil deposit but the building, through an optimization process to recreate its empirical modal properties. Two shear wall buildings were selected and simulated in a fully coupled soil-structure model to evaluate the dynamic response

of the system. Besides, two fixed base approaches are studied to compare roof displacements, interstory drifts, story shears, and accelerations.

The calibration process can be described, in general, as successful. S1D models showed that soil deposits responded in a frequency range that matched the geophysical estimation via Nakamura's method. However, buildings calibration to volumetric elements represented the main challenge. E14 modes of vibration were well recreated in modal shapes, but only if the mode had a relevant contribution in that direction. E22 modal properties remarkably matched empirical data in its first two translational modes. Regarding optimization in target natural frequencies, E22 had an excellent performance (error below 14%), while a proper estimation was reported in the first three frequencies of E14. Hence, a reasonably good match with target data was obtained in both buildings, especially in modes of vibration with an important dynamic contribution.

Based on cited studies, the type of building and foundation, soil deposit stiffness, and ground motion frequency content are fundamental aspects to assess alleged DSSI benefits. In the present investigation (shear wall type building, mat foundation, sandy soils, and synthetic inputs of broad band spectrum), the following conclusions can be made:

- Selection of adequate ground motion is critical. In this matter, the frequency content and the depth of recorded signal (e.g. FF and FIM) are extremely important for at least two reasons: input capability of exciting the system and

amplitude of the induced response. It was observed that R02-2 (lower frequency) action was stronger than R05-5 in all seismic responses.

- DSSI models had, in general, an average response between FF and FIM induced responses in uncoupled models. M2 fixation approach did not have an impact in the overall structural response.
- If drifts are corrected by the foundation slab rocking including its deformation, the fully coupled 3D model (S3D) exhibits an intermediate to lower response than fixed base models.
- DSSI generates a significant decrease in story shear envelope compared to FF action. Reported base shear increase in FF cases was up to 136% (E14) and 220% (E22).
- DSSI gives rise to significant period lengthening, which was up to 45% (E14) and 47% (E22). Spectral Ratio between building top and base suggests a decrease of roof response amplitude in all DSSI results.

Further study is required to draw general conclusions about DSSI effects in shear wall dominant buildings. Recommendations for future work include using real earthquake motions, non-linear approaches for soil and structure materials, further development in global methods of optimization as well as the inclusion of soil flexibility in building calibration. Besides, the optimized models could be validated through the comparison of predicted structural response against recorded motions in instrumented buildings.

2.8 Acknowledgements

This investigation is based on work funded partially by the FONDEF project D10E1027 and partially by CIGIDEN (National Research Center of Integrated Natural Disaster Management) FONDAP 15110017. This research was partially supported by the supercomputing infrastructure of the NLHPC (ECM-02).

REFERENCES

- Balkaya, C., Yuksel, S. B., & Derinoz, O. (2012). Soil-structure interaction effects on the fundamental periods of the shear-wall dominant buildings. *The Structural Design of Tall and Special Buildings*, 21(6), 416-430.
- Bielak, J. (1974). Dynamic behaviour of structures with embedded foundations. *Earthquake Engineering & Structural Dynamics*, 3(3), 259-274.
- Bonelli, P. (2010). Evaluación de Daños y Normativa Terremoto en Chile Central-2010. *Presentación Congreso ACHISINA*. Santiago, Chile.
- Brincker, R., Zhang, L., & Andersen, P. (2000). Modal identification from ambient responses using frequency domain decomposition. *Proceedings of the 18th International Modal Analysis Conference (IMAC)*. San Antonio, Texas.
- Calderón, J. (2007). *Update on Structural System Characteristics used in RC Building Construction in Chile*. University of Chile. Civil Engineering Thesis.
- Carpenter, L. D., Naeim, F., Lew, M., Youssef, N. F., Rojas, F., Saragoni, G. R., & Adaros, M. S. (2011). Performance of tall buildings in Viña del Mar in the 27 February 2010 offshore Maule, Chile earthquake. *The Structural Design of Tall and Special Buildings*, 20(1), 17-36.
- Comte, D., Eisenberg, A., Lorca, E., Pardo, M., Ponce, L., Saragoni, R., & Suárez, G. (1986). The 1985 central Chile earthquake: A repeat of previous great earthquakes in the region? *Science*, 233(4762), 449-453.
- Döhler, M., Andersen, P., & Mevel, L. (2017). *Variance computation of modal parameter estimates from UPC subspace identification*.
- Dutta, S. C., Bhattacharya, K., & Roy, R. (2004). Response of low-rise buildings under seismic ground excitation incorporating soil-structure interaction. *Soil Dynamics and Earthquake Engineering*, 24(12), 893-914.
- Faccioli, E., Maggio, F., Paolucci, R., & Quarteroni, A. (1997). 2D and 3D elastic wave propagation by a pseudo-spectral domain decomposition method. *Journal of seismology*, 1(3), 237-251.
- Frankel, A. (1993). Three-dimensional simulations of ground motions in the San Bernardino Valley, California, for hypothetical earthquakes on the San Andreas fault. *Bulletin of the Seismological Society of America*, 83(4), 1020-1041.

- Gade, S., Møller, N. B., Herlufsen, H., & Konstantin-Hansen, H. (2005). Frequency domain techniques for operational modal analysis. *Proc. of the 1st International Operational Modal Analysis Conference (IOMAC)*.
- Gómez, C. (2001). *Structural System Characteristics used in RC and Reinforced Masonry*. University of Chile. Civil Engineering Thesis.
- Guendelman, T., Guendelman, M., & Lindenberg, J. (1997). Bioseismic buildings profile. *Proceedings of the VII Chilean conference on seismology and earthquake engineering*.
- Guo, B., & Babuška, I. (1986). The h-p version of the finite element method. *Computational Mechanics*, 1(1), 21-41.
- Han, Y. (2002). Seismic response of tall building considering soil-pile-structure interaction. *Earthquake Engineering and Engineering Vibration*, 1(1), 57-64.
- Herlufsen, H., Gade, S., & Møller, N. (2005). Identification Techniques for Operational Modal Analysis – An Overview and Practical Experiences. *Proc. of the 1st International Operational Modal Analysis Conference (IOMAC)*.
- Instituto Nacional de Normalización. (2009). *Earthquake resistant design of buildings, Nch433 Of.1996 Mod 2009*. Santiago, Chile.
- Jacobsen, N. J., Andersen, P., & Brincker, R. (2007). Eliminating the influence of harmonic components in operational modal analysis. *Proceedings of The 25th International Modal Analysis Conference (IMAC)*.
- Jennings, P., & Bielak, J. (1973). Dynamics of building-soil interaction. *Bulletin of the seismological society of America*, 63(1), 9-48.
- Jünemann, R., de La Llera, J. C., Hube, M. A., Cifuentes, L. A., & Kausel, E. (2015). A statistical analysis of reinforced concrete wall buildings damaged during the 2010, Chile earthquake. *Engineering Structures*, 82, 168-185.
- Kausel, E. (2010). Early history of soil–structure interaction. *Soil Dynamics and Earthquake Engineering*, 30(9), 822-832.
- Komatitsch, D. (1997). Méthodes spectrales et éléments spectraux pour l'équation de l'élastodynamique 2D et 3D en milieu hétérogène (Doctoral dissertation, Institut de Physique du Globe de Paris, Paris, France). Retrieved from <https://hal-sde.archives-ouvertes.fr/tel-00007568/>

- Komatitsch, D., & Tromp, J. (1999). Introduction to the spectral element method for three-dimensional seismic wave propagation. *Geophysical journal international*, 139(3), 806-822.
- Kraus, I., & Džakić, D. (2013). Soil-structure interaction effects on seismic behaviour of reinforced concrete frames. *50 years Skopje Earthquake-50 years European Earthquake Engineering*.
- Kutanis, M., & Elmas, M. (2001). Non-linear seismic soil-structure interaction analysis based on the substructure method in the time domain. *Turkish Journal of Engineering and Environmental Sciences*, 25(6), 617-626.
- Lagos, R., Kupfer, M., Lindenberg, J., Bonelli, P., Saragoni, R., Guendelman, T., . . . Yañez, F. (2012). Seismic performance of high-rise concrete buildings in Chile. *International Journal of High-Rise Buildings*, 1(3), 181-194.
- Leyton, F., Ramírez, S., & Vásquez, A. (2012). Uso y Limitaciones de la Técnica de Microvibraciones (RHV) en la Clasificación Sísmica de Suelos. *VII Congreso Chileno de Geotecnia*. Concepción, Chile.
- Leyton, F., Ruiz, S., Sepúlveda, S. A., Contreras, J. P., Rebolledo, S., & Astroza, M. (2013). Microtremors' HVSr and its correlation with surface geology and damage observed after the 2010 Maule earthquake (Mw 8.8) at Talca and Curicó, Central Chile. *Engineering geology*, 161, 26-33.
- Li, X., Dong, L., & Zhao, Q. (2014). Seismic modelling study of P-wave attenuation and velocity dispersion in patchy-saturated porous media. *Journal of Geophysics and Engineering*, 11(6).
- Lu, X., Chen, B., Li, P., & Chen, Y. (2003). Numerical analysis of tall buildings considering dynamic soil-structure interaction. *Journal of Asian architecture and building engineering*, 2(1), 1-8.
- Magna-Verdugo, C., & Kunnath, S. K. (2014). Non-linear response analysis of reinforced concrete shear walls using multi-springs macro-models. *Proc. of the 10th National Conf. in Earthq. Eng.*
- Massone, L. M., Bonelli, P., Lagos, R., Lüders, C., Moehle, J., & Wallace, J. W. (2012). Seismic Design and Construction Practices for RC Structural Wall Buildings. *Earthquake Spectra*, 28(s1), 245-256.
- Mazzieri, I., Stupazzini, M., Guidotti, R., & Smerzini, C. (2013). SPEED: SPectral Elements in Elastodynamics with Discontinuous Galerkin: A non-conforming approach for 3D multi-scale problems. *International Journal for Numerical Methods in Engineering*, 95(12), 991-1010.

- Ministerio de Vivienda y Urbanismo. (2011). *D.S. N° 61. Building seismic design code*. Diario Oficial.
- Moroni, O., & Ghomez, C. (2002). *World Housing Encyclopedia Report*. International Association of Earthquake Engineering.
- Mylonakis, G., & Gazetas, G. (2000). Seismic Soil-Structure Interaction: Beneficial or Detrimental? *Journal of Earthquake Engineering*, 4(3), 277-301.
- Naeim, F., Tileylioglu, S., Alimoradi, A., & Stewart, J. P. (2008). Impact of foundation modeling on the accuracy of response history analysis of a tall building. *Seminar on Utilization of Strong Motion Data*, (págs. 19-55).
- Nakamura, Y. (1989). A method for dynamic characteristics estimation of subsurface using microtremor on the ground surface. *Railway Technical Research Institute, Quarterly Reports*, 30(1).
- NEHRP Consultants Joint Venture. (2012). Soil-structure interaction for building structures. *Nist Gcr*, 12-917.
- Olsen, K. B., & Archuleta, R. J. (1996). Three-dimensional simulation of earthquakes on the Los Angeles fault system. *Bulletin of the Seismological Society of America*, 86(3), 575-596.
- Paolucci, R., Faccioli, E., & Maggio, F. (1999). 3D response analysis of an instrumented hill at Matsuzaki, Japan, by a spectral method. *Journal of Seismology*, 3(2), 191-209.
- Patera, A. T. (1984). A spectral element method for fluid dynamics: laminar flow in a channel expansion. *Journal of computational Physics*, 54(3), 468-488.
- Pitarka, A., & Irikura, K. (1996). Basin structure effects on long-period strong motions in the San Fernando Valley and the Los Angeles basin from the 1994 Northridge earthquake and an aftershock. *Bulletin of the Seismological Society of America*, 86(1B), S126-S137.
- Podestá, L., Sáez, E., Yañez, G., & Leyton, F. (2019). Geophysical study and 3D modeling of site effects in Viña del Mar city, Chile. *Earthquake Spectra*.
- SARA Electronic Instruments. (2020). Retrieved from <https://www.sara.pg.it/requests/get-document.php?id=163>
- Schnabel, P. (1972). SHAKE: A computer program for earthquake response analysis of horizontally layered sites. *EERC Report 72-12*.

- Sharma, N., Dasgupta, K., & Dey, A. (2018). A state-of-the-art review on seismic SSI studies on building structures. *Innovative Infrastructure Solutions*, 3(1), 22.
- Soto, V., Sáez, E., & Magna-Verdugo, C. (2020). On the numerical modeling of 3D site-city effects including partially embedded buildings using spectral element methods. Application to the case of Viña del Mar city, Chile. *Engineering Structures*, 223, 111188.
- Stewart, J. P., & Tileylioglu, S. (2007). Input ground motions for tall buildings with subterranean levels. *The Structural Design of Tall and Special Buildings*, 16(5), 543-557.
- Stewart, J. P., Seed, R. B., & Fenves, G. L. (1998). *Empirical evaluation of inertial soil-structure interaction effects*. Univ. of California, Berkeley, CA: Pacific Earthquake Engineering Research Center.
- Stewart, J. P., Seed, R. B., & Fenves, G. L. (1999). Seismic soil-structure interaction in buildings. II: Empirical findings. *Journal of Geotechnical and Geoenvironmental Engineering*, 125(1), 38-48.
- Structural Vibration Solutions. (2019). ARTeMIS User's Manual.
- Van Overschee, P., & De Moor, B. (1996). *Subspace identification for linear systems: Theory, Implementation, Applications*. Kluwer Academic Publishers.
- Veletsos, A. S., & Nair, V. V. (1975). Seismic interaction of structures on hysteretic foundations. *Journal of the Structural Division*, 101(2), 190-129.
- Veletsos, A., & Meek, J. W. (1974). Dynamic behaviour of building-foundation systems. *Earthquake Engineering & Structural Dynamics*, 3(2), 121-138.
- Veletsos, A., & Nair, V. (1975). Seismic interaction of structures on hysteretic foundations. *Journal of the Structural Division*, 101(1), 109-129.
- Ventura, C. E., Lord, J. F., Turek, M., Brincker, R., Andersen, P., & Dascotte, E. (2005). FEM updating of tall buildings using ambient vibration data. *Proceedings of the sixth European conference on structural dynamics (EURODYN)*, (pp. 4-7).
- Wallace, J. W., Massone, L. M., Bonelli, P., Dragovich, J., Lagos, R., Lüders, C., & Moehle, J. (2012). Damage and implications for seismic design of RC structural wall buildings. *Earthquake Spectra*, 28(s1), 281-299.
- Wolf, J. P. (1985). *Dynamic soil-structure interaction*. Englewood Cliffs, NJ, Prentice-Hall.

Xu, J., Bielak, J., Ghattas, O., & Wang, J. (2003). Three-dimensional nonlinear seismic ground motion modeling in basins. *Physics of the earth and planetary interiors*, 137(1-4), 81-95.